TRIBHUVAN UNIVERSITY

INSTITUTE OF ENGINEERING

PULCHOWK CAMPUS

Preparation and Characterization of Activated Carbon from Amla (Phyllanthus emblica) Seed Stone by Chemical Activation with Phosphoric Acid for Energy Storage Devices

by

Sujan Bhandari

Thesis Number: 076MSMSE016

A THESIS SUBMITTED TO THE DEPARTMENT OF APPLIED SCIENCES AND CHEMICAL ENGINEERING
IN PARTIAL FULFILLMENT OF THE REQUIREMENTS FOR THE
DEGREE OF MASTER OF SCIENCE
IN MATERIAL SCIENCE AND ENGINEERING

DEPARTMENT OF APPLIED SCIENCES AND CHEMICAL ENGINEERING
PULCHOWK CAMPUS, IOE
LALITPUR, NEPAL

September, 2022

TRIBHUVAN UNIVERSITY

INSTITUTE OF ENGINEERING

PULCHOWK CAMPUS

DEPARTMENT OF APPLIED SCIENCES AND CHEMICAL ENGINEERING

The undersigned certify that they have read, and recommended to the Institute of Engineering for acceptance, a thesis entitled " Preparation and Characterization of Activated Carbon from Amla (Phyllanthus emblica) Seed Stone by Chemical Activation with Phosphoric Acid for Energy storage devices" (Thesis No.:076MSMSE016) in partial fulfillment of the requirements for the degree of Master of Science in Material Science and Engineering.

..…..……

Supervisor, Prof. Dr. Bhadra Prasad Pokharel

Department of Applied Sciences and Chemical Engineering

…….……

Co-Supervisor, Asst. Prof. Chhabi Lal Gnawali

Department of Applied Sciences and Chemical Engineering

..……

External Examiner

Prof. Dr.Khem Narayan Poudel

Department of Applied Sciences and Chemical Engineering

..……

Head of Department, Prof. Dr. Hem Raj Pant

Department of Applied Sciences and Chemical Engineering

2022-10-16

Date

COPYRIGHT

ABSTRACT

In order to mitigate climate change and ensure stable energy supply, energy storage is essential. Activated carbon (AC) has a large surface area which makes it ideal electrode for energy storage devices such as supercapacitors. In this work we have used Amla seeds as precursors to produce AC because of their novelty and managing agricultural waste. The AC was produced at temperatures of 400^0C, 500^0C, and 600^0C using Phosphoric acid as activating agent. Their characterization showed AC prepared at $500\ ^0$C and 600^0C had the highest surface area and amorphous contents. They also showed the comparatively high specific capacity of 0.113 Fcm^{-2} and 0.0729 Fcm^{-2} respectively for samples at temperatures 500^oC and 600^oC which means the AC prepared at these temperatures are suitable for energy storage devices.

Keywords: Activated Carbon, Electrode, Energy Storage, Energy Density

ACKNOWLEDGMENT

I wish to express my sincere gratitude to my supervisor Prof. Dr. Bhadra Prasad Pokharel, for his continuous guidance, inspiration, and encouragement during the thesis work and study period. His lectures and advice proved to be valuable in the process of this thesis work.

I would wholeheartedly like to thank my co-supervisor, Asst. Prof. Chhabi Lal Gnawali for his valuable suggestions and guidance for the thesis work. Without his suggestions, this research work could not have been of this level.

I would like to thank Prof. Dr. Sahira Joshi, our program coordinator and Prof. Dr. Hem Raj Pant, Head of Department, for providing valuable guidance throughout the progress of this thesis work. I would also like to acknowledge all the faculty members of the Department of Applied Sciences and Chemical Engineering for the knowledge and concepts they gave me during my study at IOE, Pulchowk Campus.

I would also like to thank Prof. Dr. Lok Kumar Shrestha and Asst. Prof. Tanka Mukhiya for their valuable guidance throughout the thesis work.

I would like to recognize the assistance obtained through the National Institute for Material Sciences in Japan, Nano lab and Chemistry lab of the Department of Applied Sciences and Chemical Engineering, reference books, and research papers and would like to thank their authors.

Finally, I would like to appreciate the love, support, and inspiration I got from my friends while doing this thesis work.

Sujan Bhandari

Date:2022-10-16

TABLE OF CONTENTS

Copyright 2
Abstract..... 3
Acknowledgment 4
Table Of Contents 5
List Of Tables 7
List Of Figures 7
List Of Symbols 8
List Of Abbreviations 8

CHAPTER ONE: INTRODUCTION 1
1.1 Background 1
1.2 Energy Storage 2
1.3 Supercapacitors 3
1.3.1 Types Of Scs 4
1.4 Electric Double Layer Capacitor (Edlc) 5
1.5 Electrode Of Edlc 7
1.6 Activated Carbon As An Electrode For Edlcs 7
1.7 Material 8
1.8 Synthesis Of Ac 8
1.9 Activating Agent 9
1.10 Carbonization Temperature 9
1.11 Carbonization Time 9
1.12 Chemistry Of Activation 9
1.13 Iodine Number 10
1.14 Methylene Blue Number 10
1.15 Surface Area 11
1.16 X-Ray Diffraction 11
1.17 Fourier Transfer Infrared (Ft-Ir) Spectroscopy 11
1.18 Raman Spectroscopy 12
1.19 Objectives 12
1.19.1 Main Objective 12
1.19.2 Specific Objectives 12
1.20 Assumptions And Limitations 12
1.21 Organization Of The Thesis 13

CHAPTER TWO: LITERATURE REVIEW 14
2.1 Preparation of Activated Carbon 14
2.2 Fabrication of Activated Carbon Electrode 15
2.3 Research gap 16

CHAPTER THREE: MATERIALS AND METHODS 17
3.1 Material 17
3.2 Instruments and Apparatus 17
3.3 Chemicals and Reagents 17
3.4 Method of Preparation of Activated Carbon (AC) 18
3.4.1 Washing the Sample 19
3.5 Characterization 19

3.5.1 Iodine Number 19
3.5.2 Methylene Blue Number 19
3.5.3 Surface Area 20
3.5.4 Total Pore Volume 20
3.5.5 Micropore Volume 20
3.5.6 Xray diffraction 21
3.5.7 Fourier Transform- Infrared (FTIR) Spectroscope: 21
3.5.8 Raman Spectroscopy 21
3.5.9 Scanning Electron Microscopy 21
3.6 Preparation of Electrode 22
3.6.1 Electrochemical Analysis of the electrode 22

CHAPTER FOUR : RESULTS AND DISCUSSION 24
4.1 Methylene Blue Number 24
4.2 Iodine Number 25
4.3 X-ray diffraction 26
4.4 Fourier Transform-Infrared(FTIR) 29
4.5 Raman Spectroscopy 31
4.6 Scanning Electron Microscopy 32
4.7 Surface Area 32
4.8 Micropore Volume 33
4.9 Total Pore Volume 34
4.10 Electrochemical Analysis of AC 35
4.10.1 Discussion 39

CHAPTER FIVE : CONCLUSION AND RECOMMENDATION 40
5.1 Conclusion 40
5.2 Recommendation For Future Work 40

REFERENCES 41
APPENDIX 51

LIST OF TABLES

Table 1: Overview of results of characterizations 24
Table 2: Crystalline size of sample prepared at 400 degrees.....27
Table 3: Crystalline size of sample prepared at 500 degrees.....28
Table 4: Crystalline size of sample prepared at 600 degrees.....28

LIST OF FIGURES

Figure 1: World Primary Energy Consumption by Source 1965-2021 (Ritchie et al., 2020).....2
Figure 3: Ragone plot for different energy storing devices(Liu et al., 2020) 4
Figure 4: Types of Supercapacitors(Oyedotun, 2018).....5
Figure 5: Different Models of EDLCs a)Helmholtz model b) Gouy-Chapman model c) Stern Model(Tyagi & Gupta, 2015) 6
Figure 6:Pores of Activated Carbon(Shiratori et al., 2009).....7
Figure 7: Overview of the research work 23
Figure 8: Methylene Blue Number of Carbon at different carbonization temperature25
Figure 9: Iodine Number of different samples at different temperature of activation.26
Figure 10: XRD patterns of Activated Carbon at different temperatures.....27
Figure 11: Maximum Intensity in XRD patterns of carbon for different temperatures. 29
Figure 12: FTIR spectra of all the carbon samples.....30
Figure 13: Raman Spectroscopy of the different samples of AC 31
Figure 14 A1 32
Figure 15 A2 32
Figure 16 A3 32
Figure 17: Surface Area of the ACs at different temperature of carbonization.....33
Figure 18: Micropore Volume of ACs at different temperature of carbonization.....34
Figure 19: Total Pore Volume of different ACs at different temperature of carbonization. 35
Figure 20 Voltammogram of S_{400}, S_{500}, S_{600} at 5 mVs^{-1}scan rate.....36
Figure 21 Voltammogram of S_{400} 37
Figure 22 Voltammogram of S_{500} 37
Figure 23 Voltammogram of S_{600} 38

LIST OF SYMBOLS

H_2	Hydrogen
N_2	Nitrogen
H_3PO_4	Phosphoric Acid
$ZnCl_2$	Zinc Chloride
KOH	Potassium Hydroxide
MB_N	Methylene Blue Number
mins	Minutes
PVDF	Polyvinylidene Diflouride
PS-Ac	Shrimp shell Activated Carbon
g/L	Grams per liter
IN	Iodine Number
^0C	Degree Celsius

LIST OF ABBREVIATIONS

nm	Nanometer
EDLC	Electric Double Layer Capacitor
SC	Supercapacitor
CV	Cyclic Voltammetry
rpm	Rotation per minute
cm	Centimeter
AC	Activated Carbon
mg	Milligrams
ml	Milliliter
gm	Gram
XRD	X-ray Diffraction
FTIR	Fourier Transform Infrared
MB	Methylene Blue

CHAPTER ONE: INTRODUCTION

1.1 Background

In our daily lives we use energy in various ways. From smartphones to lightning to using equipment heavy or light, we are dependent on energy, which is why energy is without a doubt our most important resource. A rapidly growing economy and rising living standards are all due to innovation in energy usage. Energy isn't just needed for business; it's vital to our survival(Pani et al., 2022).

The changes in our usage and sources of energy have been astounding. The industrial revolution which began more than 250 years ago ushered in a revolution in energy usage. Coal triggered this huge shift which was the main source of energy then. With the passing of time, oil and gas also gained prominence and became a key face in energy sources. The love for these sources still remains. Nonetheless, numerous more energy sources have been recorded, including hydro, solar, nuclear, wind, geothermal, biogas, and wave(Ahmad & Zhang, 2020). Although their usage is very limited, their rapid growth over the past few years shows they will prove to be an integral part of our energy mix shortly. These energy sources are clean as well as renewable in the sense that hydrocarbons are finite and their use harms us and the environment as well. Hence, it is necessary to move to clean and sustainable energy sources from non-renewable ones to continue economic growth and stop environmental deterioration. Renewable resources have not been effectively utilized despite their huge benefits for a variety of reasons. The causes might be due to technical limitations, high startup costs, or political pressure. While the wealthy nations have been too sluggish and hesitant to transmit their technology owing to the greater cost and political reasons, the least developed and emerging countries also confront technical backwardness and hurdles. Some of these issues are related to politics, finances, and willpower but the most important technical issue is that resilient and cheap energy storage options that are still in development(Arto et al., 2016) .

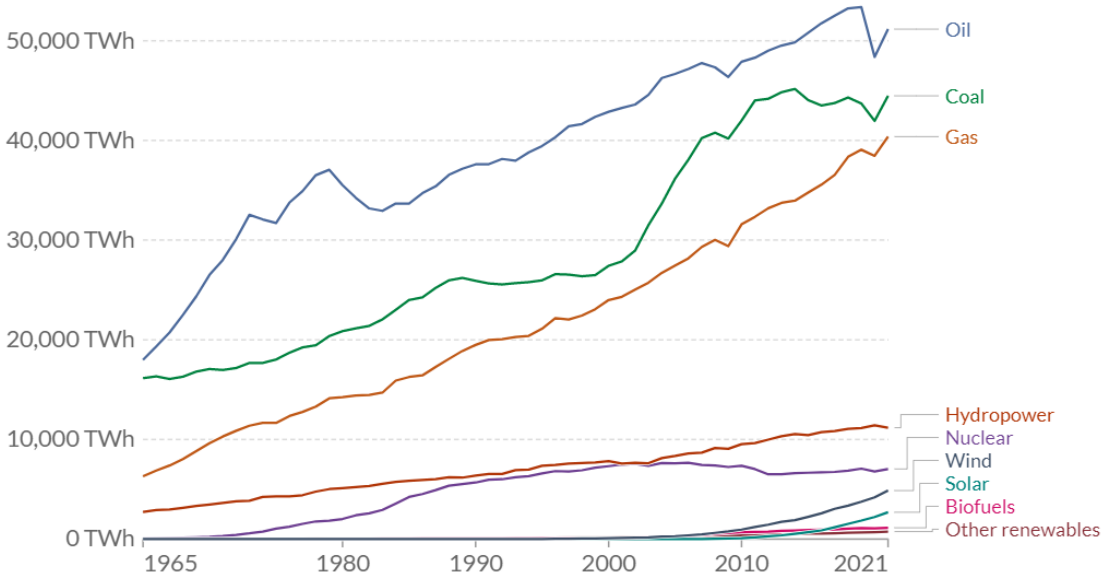

Figure 1: World Primary Energy Consumption by Source 1965-2021 (Ritchie et al., 2020)

1.2 Energy Storage

Scientists and politicians are increasingly focusing on energy storage options because of growing worries by the public about the effects of fossil fuels on the environment as well as the capacity and resilience of electricity systems worldwide. Energy storage can help address the erratic nature of solar and wind energy. Additionally, it often can react fast to substantial shifts in demand, enhancing grid responsiveness and reducing the need to build backup power plants. The efficiency of an energy storage facility is based on the pace at which energy is wasted throughout the storage process, the ability to adjust for fluctuations in demand, the total amount of energy it can store, and the speed at which it can be recharged. Energy storage devices serve as a reservoir for the electrical system, storing surplus energy produced during periods of high production and releasing it when needed (Gallo et al., 2016).

There are several techniques to store energy, each having its advantages and disadvantages. Though energy storage options like pumped-storage power is often used for large-scale energy operations, we also need portable small-scale storage options like batteries and supercapacitors (SCs).

There are two essentially different ways that electrical energy may be stored:

(1) indirectly in batteries as potentially available chemical energy requiring the electrochemically active substances to undergo faradaic oxidation and reduction so they can release charges that can carry out electrical work when they are in contact with two electrodes having various electrode potentials and
(2) electrostatically, as opposing electric charges on a capacitor's plates, a method known as non-faradaic electrical energy storage (Frackowiak, 2013).

The most fundamental difference between these two is that chemical changes are involved in the faradic process while it is not involved in the non-faradaic process. No electron transfer takes place in a non-faradaic process (Yu et al., 2017).

Although capacitors have low energy density; with high surface area and double layers, the capacitance can be increased significantly. Supercapacitors are one such energy storage device with a high capacitance value(Olabi et al., 2021).

1.3 Supercapacitors

Supercapacitors (SCs) are electrochemical energy storage devices that store and release energy by reversible adsorption and desorption of ions at the interfaces between electrode materials and electrolytes(Q. Li et al., 2014). SCs have an advantage over traditional batteries in the sense that SCs have a high specific power. They can deliver energy quicker, have a long service life, and have excellent temperature performance. In terms of storing or delivering electric charge, SCs can be compared to rechargeable batteries, although their process of charge storage is different from that found in batteries. As a result, SCs shouldn't be seen as a substitute for batteries but rather as an additional kind of energy storage that fills a specific power and energy need(Beguin & Frackowiak, 2013). The specific energy and specific power ranges of SCs may span many orders of magnitude with the right cell design, making them incredibly adaptable as a stand-alone energy source for some applications or in conjunction with batteries as a hybrid system. This special mix of strong specific energy and high-power capabilities enables SCs to position as a transitional system between batteries and conventional capacitors (Liu et al., 2020).

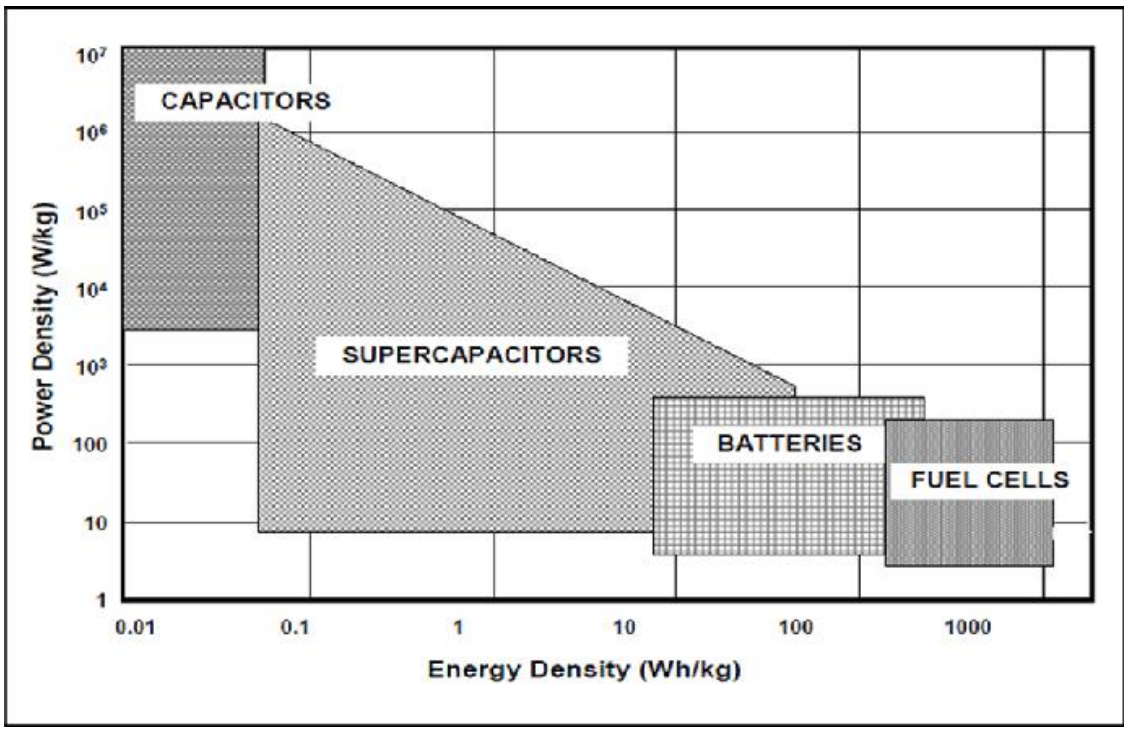

Figure 2: Ragone plot for different energy storing devices(Liu et al., 2020)

1.3.1 Types of SCs

The main function of a supercapacitor is to store energy by dispersing charged ions in the electrolyte on the electrode surfaces. The electrical double-layer capacitor, the first kind of supercapacitor, allows for reversible ion electrostatic accumulation on a porous electrode's surface. Carbon compounds with a wide surface area fall into this group. Second, the reversible redox process involving electrolyte ions and surface functional groups is a component of the pseudocapacitor category. The third type of capacitor is a hybrid capacitor, which combines an electrode similar to that of an electrical double-layer capacitor with an electrode similar to that of a faradaic battery(Shafiei et al., 2021).

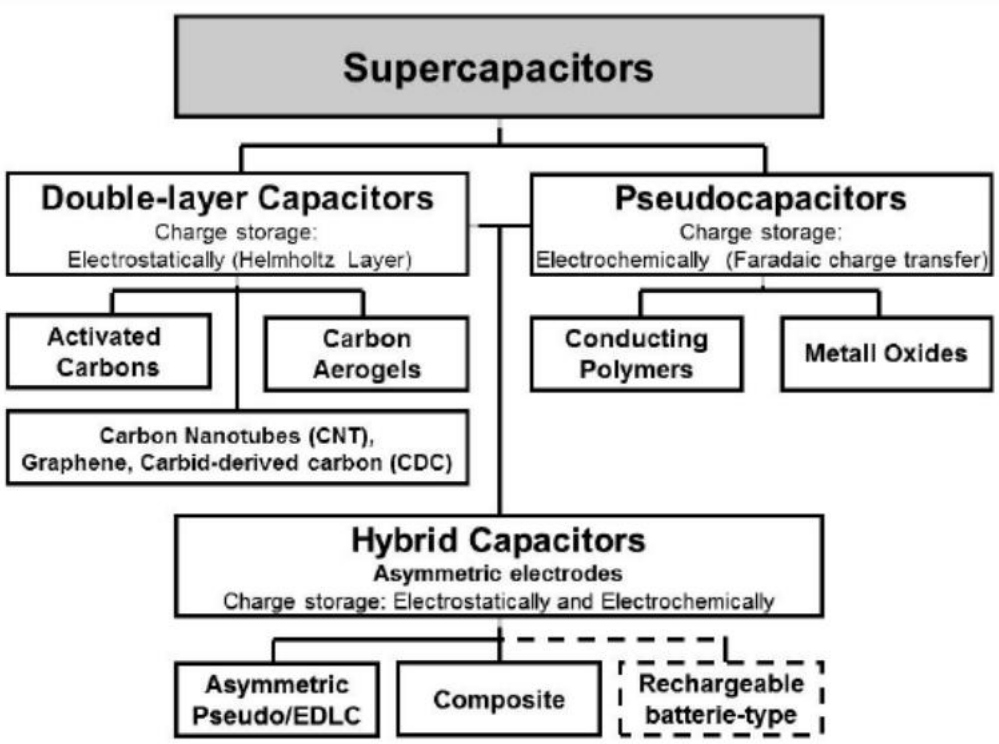

Figure 3: Types of Supercapacitors(Oyedotun, 2018)

1.4 Electric Double Layer Capacitor (EDLC)

Since von Helmholtz created and modeled the double-layer notion in his work on colloidal suspensions in the nineteenth century, the idea of the double layer has been researched by chemists(Rajapaksha et al., 2022).

According to the Helmholtz double-layer model, two oppositely charged layers separated by an atomic distance form an electrode-electrolyte interface(Pandolfo et al., 2013). In the late nineteenth and early twentieth century, this concept was further expanded to include the surface of metal electrodes. Stern merged the Helmholtz model with the more accurate Gouy-Chapman model and acknowledged that there are two areas where ions are distributed at the electrode-electrolyte interface. They are:

- Inner region called compact layer (or stern layer)
- Diffuse layer

In the diffuse layer, anions and cations are continuously distributed in solution and are driven by thermal motion as opposed to the compact layer, where ions (often solvated) are heavily adsorbed by the electrode(Tyagi et al., 2022).

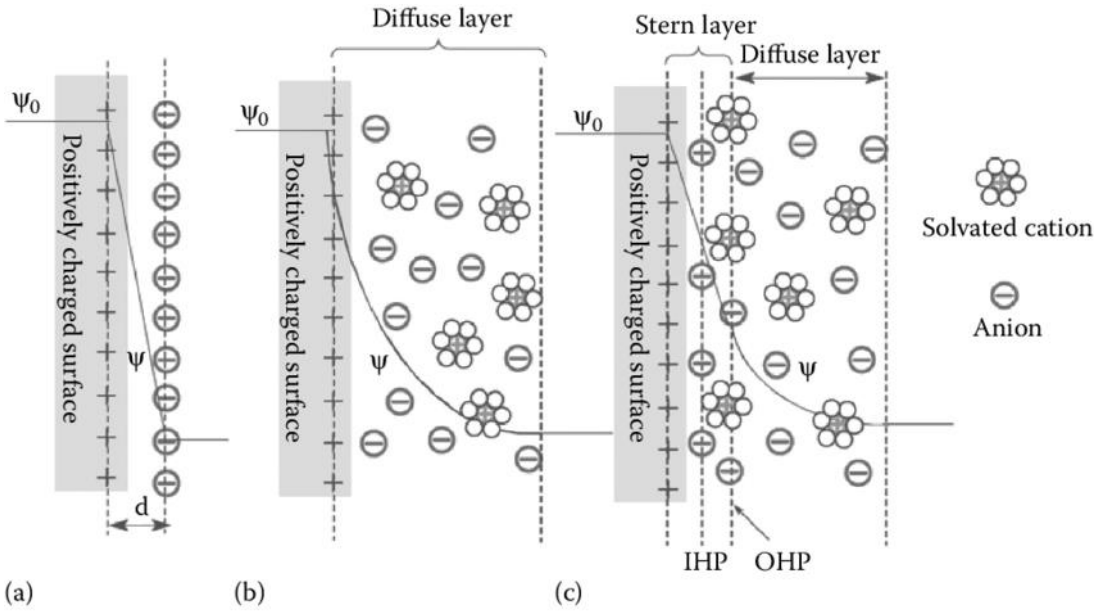

Figure 4: Different Models of EDLCs a)Helmholtz model b) Gouy-Chapman model c) Stern Model(Tyagi & Gupta, 2015)

Hence, the capacitance at the electrode-electrolyte interface double layer (C_{dl}) has two components i.e., compact double layer capacitance C_H And diffuse layer capacitance C_{diff}. The overall capacitance is hence given by the relation (Helseth, 2021)

$$\frac{1}{C_{\mathrm{dl}}} = \frac{1}{C_{\mathrm{H}}} + \frac{1}{C_{\mathrm{diff}}}$$

Eq.(1)

The capacitance of the EDLCs is determined by the electrode material (conducting or semiconducting), electrode area, accessibility to the electrode surface, the electric field across the electrode, and electrolyte/solvent properties (i.e., their interactions, size, dipole moments, etc)(Ratajczak et al., 2019).

Since the electrode material in EDLCs is frequently quite porous, the behavior of the double layer at the pore surface is more complicated. The double layer's dimensions can be equivalent to the effective pore width in extremely small pores, which means that when the diffuse layer is extended into the pore, diffuse layers from opposing surfaces may overlap and cause the ions in the diffuse layer to be redistributed(Beguin & Frackowiak, 2013).

1.5 Electrode of EDLC

EDLCs benefit from the numerous and frequently mentioned characteristics of carbon materials, such as their availability, low to moderate cost, and good electrical conductivity. The ultimate performance of carbon-based supercapacitors in EDLCs will be tightly correlated with the chemical and physical properties of the graphite electrodes(Shafiei et al., 2021).

1.6 Activated Carbon as an electrode for EDLCs

The most used material in the form of active material in commercial EDLCs is Carbon. A unique mix of strong conductivity and extremely high surface area makes AC incomparable. In addition to this, stable supply and well-established fabrication procedures make ACs attractive materials for EDLC preparation. The pores in AC are of different types and provide the surface for ions. The pores range from visible to nanometer in dimensions. According to the IUPAC (International Union of Pure and Applied Chemistry), three groups of pores are distinguished, according to the pore size:

- Macropores (> 50 nm diameter)
- Mesopores (2-50 nm diameter)
- Micropores (< 2 nm diameter) (L. Li et al., 2002)

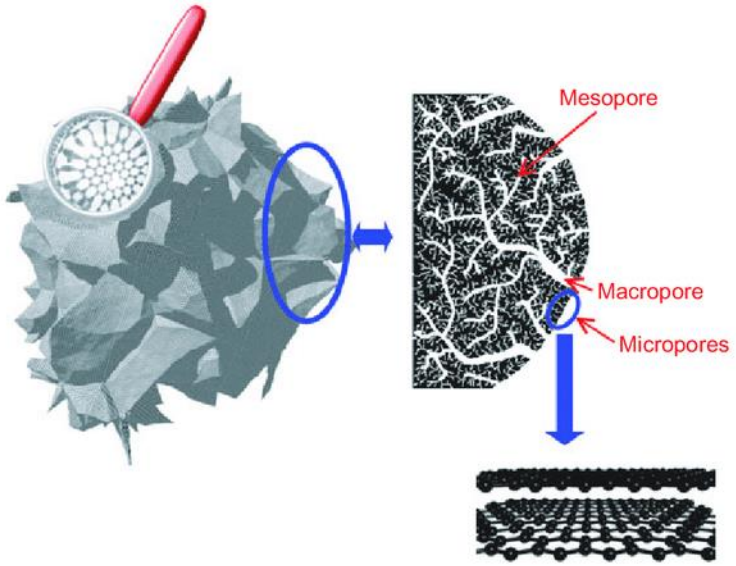

Figure 5:Pores of Activated Carbon(Shiratori et al., 2009)

Due to the effective adsorption of electrolyte ions, micropores are the main source of capacitance. Mesopores and macropores provide channels for ions to reach micropores. Activated carbons with high surface areas and acceptable pore size distributions are more likely to exhibit very good electrochemical performance. Therefore, activated carbons with micropores optimized for capacitance and an appropriate amount of mesopores for high capacity performance are highly desirable for EDLCs. (Ma et al., 2021).

Physical or chemical activation processes can be used to create porous activated carbon. Physical activation generally requires high temperature hence we used chemical activation using phosphoric acid for the AC synthesis(Williams & Reed, 2006).

There are many studies to prepare activated carbon using a precursor of biomass of wheat, corn straw, olive stones, Lapsi seeds, etc (Joshi, 2017; Yahya et al., 2015). This research aims to use a locally abundant novel biomass-based precursor of amla seeds native to our area and activated using easily available phosphoric acid. Though the application of AC is diverse we will use it as an electrode for energy storage applications.

1.7 Material

Amla (Phyllanthus emblica) is a deciduous tree found in South Asia. It is used mainly as a medicinal plant(Saini et al., 2022). In this thesis, seed stones of amla are used as a lignocellulosic precursor to produce Activated Carbon. Lignocellulose refers to the biomass of plants containing cellulose, hemicellulose, and lignin(Mehta et al., 2020). Amla was chosen as the precursor because of its nativity to our area, managing agricultural waste during medicine preparation and the lack of literature on the production of activated carbon using this material is virtually nonexistent.

1.8 Synthesis of AC

AC can be made from carbonaceous material by carbonization in an inert atmosphere and then activating the carbonized product. The process of carbonization produces fixed carbon with a simple pore structure. The pores' width increases during activation and new pores are also produced. There are two categories of activation techniques: chemical and physical(Naji & Tye, 2022). Physical activation is done in two steps: carbonization and activation utilizing high-temperature oxidizing gases like carbon dioxide and steam. On the other hand, chemical activation just requires one step (Joshi,

2017). In this procedure, a dehydrating agent is used to activate the precursor before carbonization in an inert environment. Lower carbonization temperatures, improved pore structure, and high product yield are major benefits of chemical activation over physical activation.

1.9 Activating Agent

In chemical activation processes, well-known chemical agents, i.e., $ZnCl_2$, H_3PO_4, H_2SO_4, NaOH, KOH, and K_2CO_3, are used to activate carbons, resulting in a high surface area and appropriate porous. structure (Yahya et al., 2015). The most used activating agent for the synthesis of activated carbon is H_3PO_4, $ZnCl_2$, and KOH. In this work, we use Phosphoric acid as an activating agent because zinc chloride activation causes problems such as corrosion, inefficient chemical recovery, and environmental disadvantages(Husien et al., 2022). Also, KOH as an activating agent requires a high temperature for activation(Karapınar, 2022).

1.10 Carbonization Temperature

The temperature at which Activated carbon is called Carbonization temperature. As carbonization temperatures increase, the surface area of AC products increases and AC yields decrease. This can be attributed to the volatilization process (Lim, 1996). The lignocellulosic precursors must undergo a thorough chemical transformation into graphene structures at a minimum carbonization temperature of 400 °C(Veeramani et al., 2017).

1.11 Carbonization Time

During the carbonization process, the carbonization period should be long enough to allow the development of porosity in AC and volatiles from the precursor. However, if the carbonization process takes too long, the pores widen and the surface area decreases(Üner & Bayrak, 2018).

1.12 Chemistry of Activation

The precursors for preparing ACs are lignocellulosic or cellulosic in nature. It has been shown that the impregnation ratio which is the ratio of the weight of the impregnant to the precursor, and the activation temperature control the characteristics of the resulting activated carbons(Jagtoyen & Derbyshire, 1993).

Phosphoric acid-impregnated particles take on an elastic quality. The acid separates the cellulose fibres and partly depolymerizes lignin and hemicellulose (the main components of the matrix). As a result, mechanical resistance is reduced. The particle swells because of these effects. Due to the substantial quantity of tar that can be seen on the surface of the particles, impregnation also initiates carbon conversion. Tars are created when phosphoric acid catalysed depolymerization of cellulose occurs, which is then followed by dehydration, condensation, and the production of further aromatic and reactive chemicals with some cross-linking (Solum et al., 1995). The presence of phosphates may cause further cross-linking to occur. Even if the structure of carbon impregnated at low impregnation ratios resembles char, increasing acid concentrations show a more obviously damaged surface. The original cellular form of the precursor is lost because a substantial component of the cellulose structure has been taken from the inside to the outside of the particle and destroyed at high concentrations (Figueiredo et al., 1999).

During heat treatment, H_3PO_4 has a drying effect on the inside of the particles i.e. components of cellulose, hemicellulose, and lignin. Because the chemical is a liquid at the process temperature, the bonding to the precursor is thermally destroyed, resulting in dehydration. All pore sizes grow in proportion to the increased volume of micropores caused by the phosphoric acid-induced widening of microporosity, resulting in activated carbons with different micropore volumes but the same micropore size distribution (Marsh & Reinoso, 2006).

1.13 Iodine Number

The iodine number (IN), used to determine surface area by iodine adsorption on carbon, shows the amount of micro-pore dispersion in the carbon. To find the iodine number, the amount of iodine adsorbed by one gram of carbon is measured in milligrams (Nunes & Guerreiro, 2011). The iodine number and surface area are related. The iodine number was determined according to the standard method (Haimour & Emeish, 2006).

1.14 Methylene Blue Number

The Methylene Blue Number (MB_N), which is also used to calculate surface area, reveals the amount of mesopore dispersion in the carbon. The greatest quantity of methylene blue dye that may be absorbed by 1 g of adsorbent measured in mg gives the

MB_N. MB_N of the AC was determined by single point adsorption isotherm method according to procedure (Raposo et al., 2009).

1.15 Surface Area

The Surface area of ACs is mainly measured using the Brunauer-Emmett-Teller (BET) method(Mianowski et al., 2007). The approximate surface area can be determined by the adsorption of iodine and methylene blue dye (Nunes & Guerreiro, 2011). The iodine number gives an approximate measure of the micropore content while the methylene blue number gives mesopores content in the AC. This method does not require sophisticated equipment, hence is less expensive. It is considered a simple, easy, and quick method for evaluating the surface area of micro and mesopores carbons(Şahin et al., 2015).

1.16 X-Ray Diffraction

An X-ray diffraction technique determines a crystal's structure by analyzing how the structure of a crystal causes an X-ray beam to diffract in several different directions. Cathode ray tubes produce X-rays, which are then focused and collimated to produce monochromatic radiation before being directed onto materials. Using measurements of the angles and intensities of these diffracted beams, crystallographers can estimate the electron density within a crystal in three dimensions. In addition to their chemical bonds and crystallographic disorder, this electron density also provides information about the mean position of the atoms in the crystal. Identification of unknown crystalline materials (such as minerals and inorganic compounds) is widely performed by using this technique. X-ray diffraction technique is essential for studies in geology, environmental science, materials science, engineering, and biology to determine unknown solids(Ali et al., 2022).

1.17 Fourier Transfer Infrared (FT-IR) spectroscopy

Fourier transform infrared (FT-IR) spectroscopy is used for further characterization of activated carbon as well as synthesized composite particles. The functional groups present at the surface of activated carbon can be identified by this analysis(Mozhiarasi & Natarajan, 2022). This technique is very widely used in which the data is collected and converted from an interference pattern to a spectrum(Berthomieu & Hienerwadel, 2009).

1.18 Raman Spectroscopy

One of the most effective methods for characterizing carbon-based materials is Raman spectroscopy since the spectral shape demonstrates a broad range of variation that corresponds to the forms of carbon and reveals minute structural details(Staveley, 2016).

1.19 Objectives

The objective of this research work is classified into main and specific objectives as below

1.19.1 Main Objective

- To synthesize and characterize the activated carbon from Amla (Phyllanthus emblica) seed stones and use it for energy storage applications.

1.19.2 Specific Objectives

The specific objectives include:

- To synthesize Activated Carbon from Amla seed Stones using Phosphoric Acid as an activating agent at temperatures 400 ^{o}C,500 ^{o}C, and 600^{o}C
- To characterize AC using XRD, FTIR, Methylene Blue, Iodine Number, and Surface Area.
- To prepare the electrode using the synthesized AC and perform the electrochemical characterization.

1.20 Assumptions and Limitations

The assumptions of the research work were:

- The synthesized AC with the highest surface area lies within the temperature range of 400 ^{o}C to 500 ^{o}C.
- The synthesized AC has high specific capacitance and can be used as an electrode for supercapacitors.

The limitations of the research work were:

- There is a time constraint for performing the characterizations, most of which are not available in our country.
- The instrumentation and working of the electrochemical workstation require experts in the field.

1.21 Organization of the thesis

The thesis report consists of six chapters as follows:

Chapter One- Introduction: This chapter consists of the introduction to the related terminologies, statement of problems and objectives of the report

Chapter Two- Literature Review. It deals with the relevant literature for this report work.

Chapter Three: Methods and Methodologies: In this chapter, the materials and methods used in the experiments are described and the characterization techniques have been mentioned.

Chapter Four: Result and Discussion: The analysis of the results is presented in this chapter along with the figures related to characterization, morphology, Structural properly and efficiency of the prepared Activated carbons.

Chapter Five- Conclusions and Recommendation: The conclusion of the report is mentioned here, and future recommendation of the research work has also been highlighted.

The images related to the topic are given in the appendix.

2 CHAPTER TWO: LITERATURE REVIEW

2.1 Preparation of Activated Carbon

Heidarinejad et al., (2020) found that low-temperature activation with phosphoric acid is frequently utilized for lignocellulosic material. Despite producing a larger surface area than phosphoric acid, zinc chloride is utilized less frequently due to environmental issues. In comparison to potassium hydroxide, potassium carbonate generates more AC and has a larger surface area for the adsorption of big pollutant molecules like dyes. In terms of surface area and effectiveness, potassium hydroxide activation produces superior results than sodium hydroxide for a variety of applications.

Liu et al. (2018) produced a net-like porous activated carbon using shrimp shell waste as a new precursor by solution-processed carbonization and chemical activation with phosphoric acid (H_3PO_4). It demonstrated that PS-Ac was a porous substance with mesoporous structures.

Han et al., (2020) prepared AC by thermally activating eucalyptus residue that had been treated with phosphoric acid. The mass ratios of phosphoric acid and eucalyptus residue as well as the activation temperature might be used to modify and regulate the textural characteristics and acidic functional groups of the activated carbon. Additionally, they discovered that by changing the adsorption pattern from planar to side adsorption with a drop in activation temperature, acidic functional groups might improve MB adsorption.

Joshi, (2016) used zinc chloride as an activating agent for the preparation of AC from lapsi seed and measured the value of iodine number and methylene blue number and found that on increasing the temperature the methylene blue number and iodine number increased gradually implying that the pore concentration of the AC increased with increasing temperature.

Mallick et al., (2019) prepared AC from Date (Phoenix dactylifera) seeds using KOH as an activating agent from 400 to 700 °C. AC prepared at 700°C had a high degree of porosity and was suitable for use of dye adsorption and wastewater treatment technology.

Joshi et al., (2015) synthesized AC from Lapsi seed stone activated by Sodium Hydroxide at different impregnation ratios and found that the impregnation ratio of the sodium hydroxide is an important parameter for the preparation of AC.

Rajabathar et al., (2020) prepared AC from cow dung using phosphoric acid as an activating agent at a temperature range of 600 to 900 °C and found it to have a very high specific capacitance value of 2457 m^2/g at 900 °C with improved cyclic stability.

2.2 Fabrication of Activated Carbon Electrode

Sivachidambaram et al., (2017) prepared phosphoric acid activated carbon from Borassus flabellifer flower (BFF) at activation temperatures 600, 700, 800, and 900 °C. As the temperature of the activation increased the specific surface area increased. At 900 °C the AC had BET specific surface area of 633.43 $m^2\ g^{-1}$ and the X-ray diffraction patterns confirmed the amorphous nature of the activated carbon samples. Moreover, electrochemical measurements also showed that this sample can be used as electrode material for EDLCs.

Chen et al., (2013) synthesized AC from the cotton stalk and phosphoric acid as an activating agent with a mass ratio of 1:4 at an activation temperature of 800 °C for 2 hours. With these experimental conditions, activated carbon with a BET surface area of 1,481 $cm^2\ g^{-1}$ and capacitance of the prepared activated carbon was as high as 114 Fg^{-1}

Shrestha & Rajbhandari, (2021) synthesized AC from wood dust of Shorea robusta using different activating agents; H_3PO_4, KOH, and Na_2CO_3 and characterized them. The surface area of AC formed by Phosphoric acid was found highest at 1269.5 m^2/g. The specific capacitance and cyclic stability were also highest for this sample.

Du et al., (2017) prepared AC through carbonization of Enteromorpha prolifera. The prepared AC was fabricated in supercapacitor electrodes with the capacitance of 180 F g^{-1} but was less than polyaniline composite electrodes having a capacitance of 622 Fg^{-1}

Zeng et al., (2021) used eucalyptus carbon (EC) to produce eucalyptus-activated carbon (AC) through a unique technique of using phosphoric acid (H_3PO_4) and tested the resulting material for its effectiveness in removing Cr (VI) from aqueous environments. They discovered that the surface area of AC rose by almost 5 times 1265.56 m^2/g compared to EC (253.25 m^2/g).

Ozpinar et al., (2022) used a one-step chemical activation to create activated carbon from hazelnut-shell wastes. Specific capacitance values of the magnetic-activated carbon electrode and 247.8 F g^{-1} and 76.23 F g^{-1} at 0.75 A g^{-1}, respectively. The activated carbon's greater capacity to adsorb mobile ions was proved by its higher constant phase element coefficient. The findings demonstrated that activated carbon electrodes for energy applications have greater capacitive performance.

2.3 Research gap

To solve a global problem, we must be using local resources. Research regarding supercapacitor electrode fabrication using a locally available precursor of amla was virtually nonexistent. This research aims to fill this gap to learn the energy storage properties of AC prepared from locally available Amla seed stones. This research hopes to produce a cheap and easy method to produce AC using amla seed stones so that it can be used for energy storage application.

3 CHAPTER THREE: MATERIALS AND METHODS

3.1 Material

Amla seeds were gathered at the Ason neighbourhood market in Kathmandu, Nepal. The Amla seeds were dried in an electric oven at 80 °C for 24 hours after being rinsed numerous times with distilled water. The dried seed stones were crushed, ground, and sieved in a sieve of 33 micrometers. The powdered precursor was mixed with phosphoric acid in the ratio of 1:1 by weight and carbonized in the horizontal tubular furnace at different temperatures in inert environment.

3.2 Instruments and Apparatus

The entire experimental study utilized the following tools.

a) Horizontal tubular furnace

The ACs were prepared in horizontal tubular furnace from Accumax India using quartz tube from K-JHIL Scientific, Gujarat having internal diameter 2.7 cm and external diameter 3 cm.

b) Spectrophotometer

The concentration of MB adsorption for Surface Area determination and MB dye removal was also measured by UV/Vis (CECIL-CE-100) Spectrophotometer.

c) pH meter

The various pH of MB solution was maintained using the Hanna pH instrument.

d) Electric shaker

The rotary shaker from Marine India was used for finding the Methylene Blue number of the AC samples.

e) Hotbox Oven

The hotbox oven from Gallenkamp India of size 1 was used for drying the precursors and wet ACs.

3.3 Chemicals and Reagents

The following chemicals were used in the research work:

- Phosphoric Acid (H_3PO_4) from Finar India
- Iodine from Thermo Fisher Scientifc India
- Potassium Iodide(KI) from Merk (India)

- potassium dichromate ($K_2Cr_2O_7$) from Fisher Scientific
- sodium thiosulphate ($Na_2S_2O_3•5H_2O$) from Fizmerck India
- Potassium hydroxide (KOH) from Fizmerck India,
- Sulphuric acid (H_2SO_4) from Fisher Scientific,
- Hydrochloric acid (HCl) from Fisher Scientific

The reagents prepared for this research work were:

a) Stock solution of methylene blue:
100 mg of methylene blue were dissolved in 1000 ml of distilled water to create a stock solution. By diluting the stock solution, the standard MB solution was created as needed.

b) 5% HCl solution:
5 mL of HCl were dissolved in 100 ml of distilled water to create 5% HCI.

c) 0.1N Iodine solution:
0.IN Iodine solution was made by combining 3.175 g of iodine with 10% KI and diluting the mixture to 250 ml with distilled water.

d) 0.1M Sodium thiosulphate:
To make 0.1M sodium thiosulphate, 6.2 g of sodium thiosulphate were dissolved in 250 ml of distilled water.

e) 1% Starch solution:
It was prepared by dissolving 1.0 gm of starch in 100 ml of distilled water which was heated to boil for 5 minutes.

3.4 Method of Preparation of Activated Carbon (AC)

Amla seeds were brought from the market and the outer part was removed and the stone was rinsed with tap water. It was dipped in an electric shaker, dipped in distilled water and the temperature was increased to 40^0C. The seed stone was then put in mixed with Phosphoric Acid; at ratio 1:1 i.e., for 15 gm of precursor 33 ml of acid was taken. The combinations were cooked on a hot plate until a somewhat dry mass was produced, and they were then put inside an oven set at 100° C for 24 hours. Separately, the dried mixes were put in a quartz tube, positioned in a horizontal tubular furnace, and

carbonised at 400 °C,500 °C ,600°C and 700° under constant nitrogen gas flow at a rate of 100 mL/min, for 4 hrs.

3.4.1 Washing the Sample

The samples were rinsed with distilled water using a funnel and filter paper. Following washing, the carbon samples were dried for three hours at 100°C in a vacuum oven. For further characterization, the samples were stored in airtight containers.

3.5 Characterization

The prepared ACs under different preparation conditions were characterized by adsorption of iodine and methylene blue, scanning electron microscopy (SEM), X-ray diffraction (XRD) and Fourier transform infrared (FTIR) spectroscopy.

3.5.1 Iodine Number

The conventional procedure was used to determine the iodine number (ASTM method, 2006). 10ml of 5% by weight HCL was poured to 1gm of the prepared AC and left to boil. 10ml of 0.1N iodine solution were added once the solution had cooled. The material was thoroughly shaken for 30 seconds before filtering. Using starch as an indicator, the whole filtrate was titrated against a 0.05M sodium thiosulphate solution.

The Iodine Number can be calculated as:

$$\text{Iodine number } (mg/g) = C \times \ Conversion\ factor$$

Eq.(2)

where C is the difference between Blank Reading and Volume of hypo solution adsorbed by AC. The formula for calculating conversion factor is given by (Nunes & Guerreiro, 2011)

$$\text{Conversion factor } = \frac{\text{Equivalent weight of Iodine } \times 10 \times \text{Normality of Iodine}}{\text{Activated carbon Mass} \times \text{ Blank reading}}$$

Eq.(3)

3.5.2 Methylene Blue Number

Methylene Blue is a synthetic amorphous dye. It is a dark green powder but in the aqueous form, it is blue in color. In water, it decomposes into Methylene Blue cation

and chloride ion. Methylene blue number (MBN) gives the amount of methylene blue dye adsorbed by 1 gram of adsorbent which is activated carbon. MBN was determined by the single-point isotherm method(Nunes & Guerreiro, 2011) in this research paper.

$$MB_N\,(mg/g) = \frac{(Co - Ce)xV}{M} \qquad \text{Eq.(4)}$$

Where, Co = initial concentration of MB solution (mg/L)

Ce = equilibrium concentration of MB solution (mg/L)

V = volume of adsorbate solution in liter & M = weight of adsorbent in g.

3.5.3 Surface Area

The surface area of activated carbon was determined by multiple regressions model using the iodine number and methylene blue numbers. The surface area of prepared AC can be calculated by using the following equation (Nunes and Guerreiro, 2011).

$$S(m^2g^{-1}) = 2.28 \times 1.01 \times 10^{-1}\text{MBN} + 3.00 \times 10^{-1}\text{IN} + 1.05 \times 10^{-4}\text{MBN}^2 + 2.00 \times 10^{4} \times \text{IN}^2 + 9.38 \times 10^{-10}\ \text{MBN IN} \qquad \text{Eq.(5)}$$

3.5.4 Total Pore Volume

The total pore volume of the sample is determined by the linear model through multiple regressions method (Nunes and Guerreiro, 2011).

$$Vt_{(cm^3g^{-1})} = 1.37 \times 10^{-1} + 1.90 \times 10^{-3}MBN + 1.00 \times 10^{-4}IN \qquad \text{Eq.(6)}$$

3.5.5 Micropore Volume

The micropore volume of the activated carbon can also be estimated through methylene blue number and iodine number by multiple regression method (Nunes and Guerreiro, 2011).

$$Vm_{(cm^3g^{-1})} = 5.60 \times 10^{-2} - 1.00 \times 10^{-3}\text{MBN} + 1.55 \times 10^{-4}IN + 7.00 \times 10^{-6}\text{MBN}^2 + 1.00 \times 10^{-7}IN^2 - 1.18 \times 10^{-7}\text{MBN}IN \qquad \text{Eq.(7)}$$

3.5.6 Xray diffraction

The prepared activated carbon from Amla seed stone were homogeneously spread on the surface of a glass slide and mounted on Beaker D_2 Phaser X-ray Diffractometer, NAST Nepal. To further calculate the crystallite size (d) we use Debye Scherrer's equation(Wang & Gu, 2022) as follows:

$$d = \frac{K \times \lambda}{\beta \times \cos\theta}$$

Eq.(8)

where K(=0.94) is the Scherrer constant

,λ is wavelength of the X-ray beam used

,β is Full width at half maximum (FWHM) of the peak in radians and

θ is the Bragg angle. Scherrer constant denotes the shape of the particle and its value is most commonly taken as 0.94. The miller indices, crystallite size, and the FWHM were found using MATCH! software.

3.5.7 Fourier Transform- Infrared (FTIR) Spectroscope:

Functional groups and fingerprint regions of the synthesized AC sample in this study were investigated using FTIR spectroscopy. A Perkin Elmer Spectrophotometer from the Department of Plant Resources, Thapathali, was used to record FTIR spectra for all samples.

3.5.8 Raman Spectroscopy

The comparatively sharp G and D bands with graphitic sp^2 sites predominate the Raman spectra of AC. The E_{2g} symmetry of the Activated Carbon's G band depicts the in-plane bond stretching of sp^2 carbon pairs. The A_{1g} symmetry of the D band , which is a breathing mode is not allowed in perfect graphite, and only becomes active in the presence of disorder such as sp^3 sites or grain edges (Das & Guo, 2022). The Raman spectroscopy was performed by Raman Spectrometer JASCO NRS 3000.

3.5.9 Scanning Electron Microscopy

SEM analysis of the AC reveals the texture and porosity of the sample. The surface morphology helps us to get idea about the physical characteristics of the sample which

in turn gives idea about the entrance to adsorbtion sites of the AC(Somasundaran, 2006).

3.6 Preparation of Electrode

For the electrode, 4 mg of AC is taken. Prepared activated carbon, carbon black, and polyvinylidene difluoride (PVDF) are mixed in the ratio of 8:1:1 by weight in isopropyl alcohol to form a homogeneous mixture. 2 drops of the mixture is pippeted in the shiny region of the working electrode(Mukhiya et al., 2019).

3.6.1 Electrochemical Analysis of the electrode

Cyclic Voltammetry: For the Cyclic Voltammetry process, we use 3 electrode system. It consists of a working electrode, a reference electrode, and a counter electrode. Silver-Siver chloride is used as a reference electrode, Platinum wire is used as a counter electrode and glassy carbon or our prepared electrode is used as a working electrode. A basic electrolyte solution of 6M KOH was prepared and put in the cell. The specific capacitance of the electrode can be calculated by the following formula (Choi, 2010):

$$C_p = \frac{A}{2km\Delta V}$$

Eq.(9)

Where A = Area of the curve k = Scan rate m = active mass of the sample used

ΔV= Potential window = ($V_2 - V_1$)

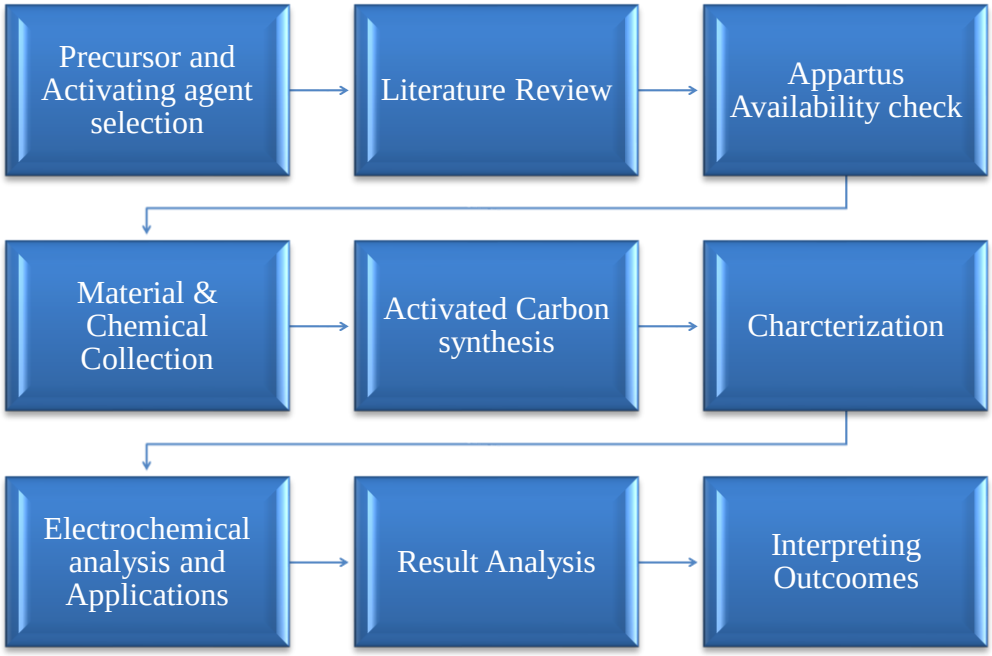

Figure 6: Overview of the research work

The overview of the complete work done for this research paper is shown in the above figure.

4 CHAPTER FOUR : RESULTS AND DISCUSSION

The characterization of the amla seed stones gave us the results for Methylene Blue number, Iodine Number, Surface Area, Total Pore Volume, FTIR, and XRD. Moreover, the electrochemical analysis of the AC gave us the result for the specific capacitance using the Cyclic Voltammetry technique.

Table 1: Overview of results of characterizations

Sample	Temperature (^oC)	Methylene Blue Number	Iodine Number	Surface Area	Meso pore Volume	Total Pore Volume
S_{400}	400	249	750.43	722.39	0.39	0.68
S_{500}	500	307	842.58	844.28	0.57	0.81
S_{600}	600	291	831.42	822.12	0.53	0.77

4.1 Methylene Blue Number

One quick and simple test method for determining the porous structure of mesoporous carbon is Methylene Blue adsorption. Methylene Blue Number gives information regarding mesopore distribution of AC. As shown in the graph below, the (S_{500}) sample of AC prepared at 500° C had a better mesopore distribution compared to the other two samples since it has a methylene blue number of 307 mg/g and the samples (S_{400} and S_{600}) have MB_N of 249 and 291 mg/g respectively.

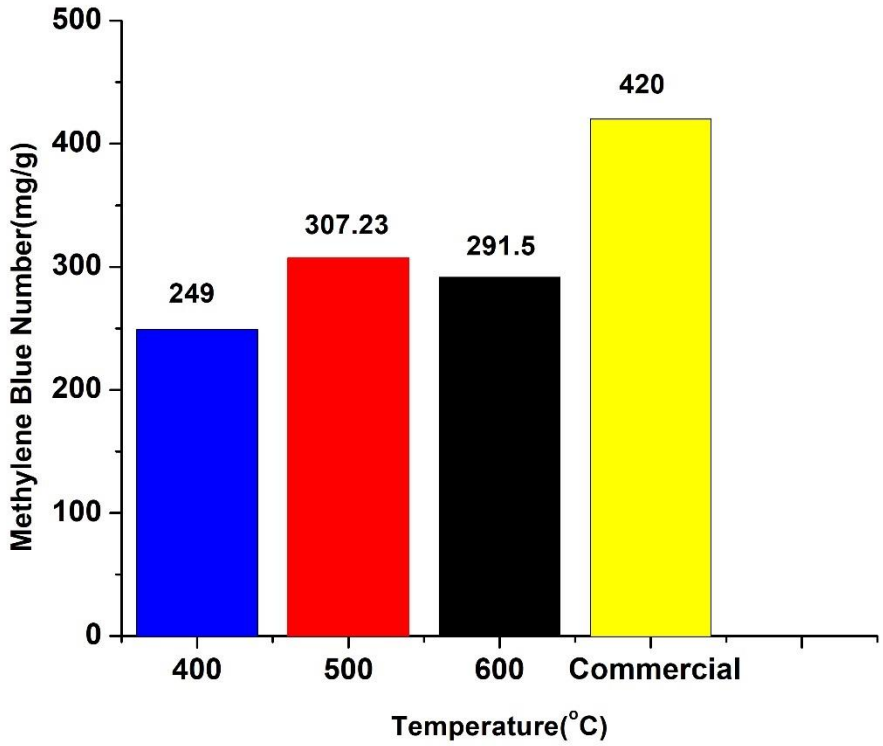

Figure 7: Methylene Blue Number of Carbon at different carbonization temperature

4.2 Iodine Number

The porous structure of micro carbons may be assessed quickly and easily using the iodine number test technique. Due to the high molecular linear size of MB, it is often employed to assess the dye removal capacity of ACF or to analyze the pore structure with a pore size of more than 1.5 nm on the surface of the adsorbent. Additionally, iodine molecules have spherical shapes with diameters of around 0.54 nm, and adsorption takes up an area of at least 0.39 nm2. As a result, iodine adsorption is typically utilized to characterize the micropores in porous materials. (Ma et al., 2019)

The graph shows the iodine number at different temperatures. At 500^0C, we have the highest iodine number of 842.58 mg/g for sample S_{500}. Similarly, samples S_{400} and S_{500} have the iodine number of 750.43 mg/g and 831.42 mg/g respectively.

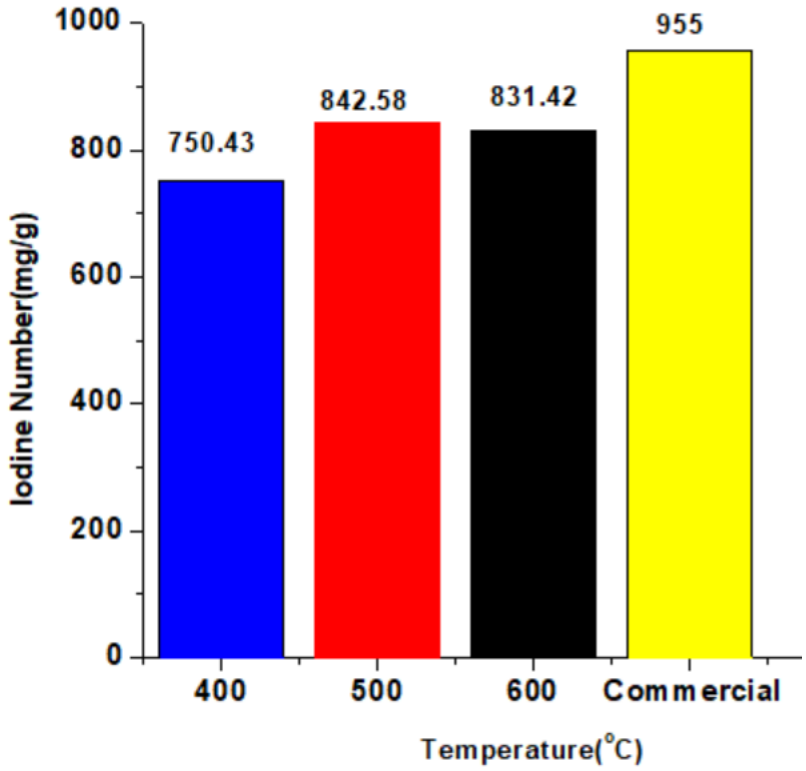

Figure 8: Iodine Number of different samples at different temperature of activation

4.3 X-ray diffraction

The figure shows the X-ray diffraction patterns of the activated carbon prepared at 400°C, 500°C, and 600°C. The peaks centered at around 26 and 42 degrees correspond to the (002) and (001) planes. It shows that the Activated Carbon is composed of graphite crystallites. The crystallite size for the samples (S_{400}),(S_{500}), and (S_{600}) was found using the Scherrer equation to be 215°A,95.05°A, and 132.07 °A.

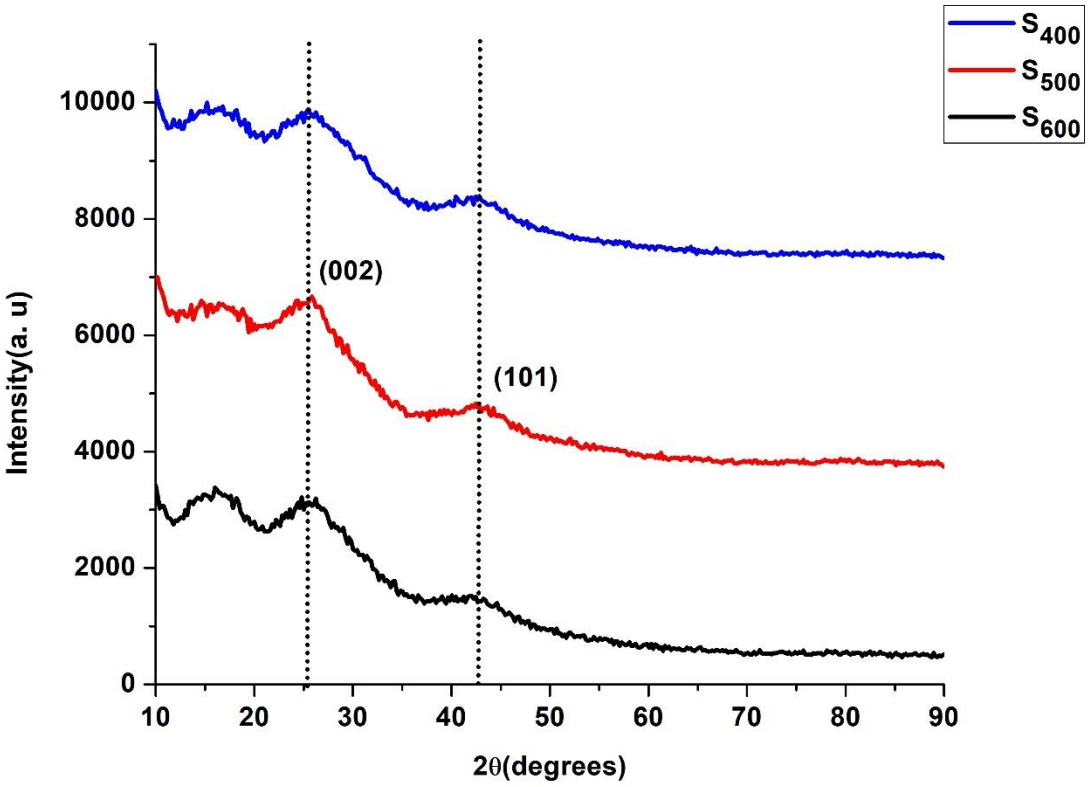

Figure 9: XRD patterns of Activated Carbon at different temperatures

Table 2: Crystalline size of sample prepared at 400 degrees

$2\theta(^{o})$	d(Å)	FWHM(rad)	Crystallite Size(Å)	Average crystalline size (Å)
16.913	5.238	0.6009	139.6	215
25.927	3.433	1.4002	60.7	
42.652	2.118	0.2003	444.7	

Table 3: Crystalline size of sample prepared at 500 degrees

2θ(degrees)	d(Å)	FWHM	Crystallite Size(Å)	Average Crystalline Size (Å)
17.91	4.975	1.0015	83.9	95.05
25.73	3.460	0.8012	106.2	
43.05	2.099	-	-	

Table 4: Crystalline size of sample prepared at 600 degrees

2θ	d(Å)	FWHM	Crystallite Size(Å)	Average Crystalline Size (Å)
17.11	5.177	0.8012	104.7	132.7
26.23	3.395	1.2019	70.9	
42.85	2.108	0.4006	222.5	

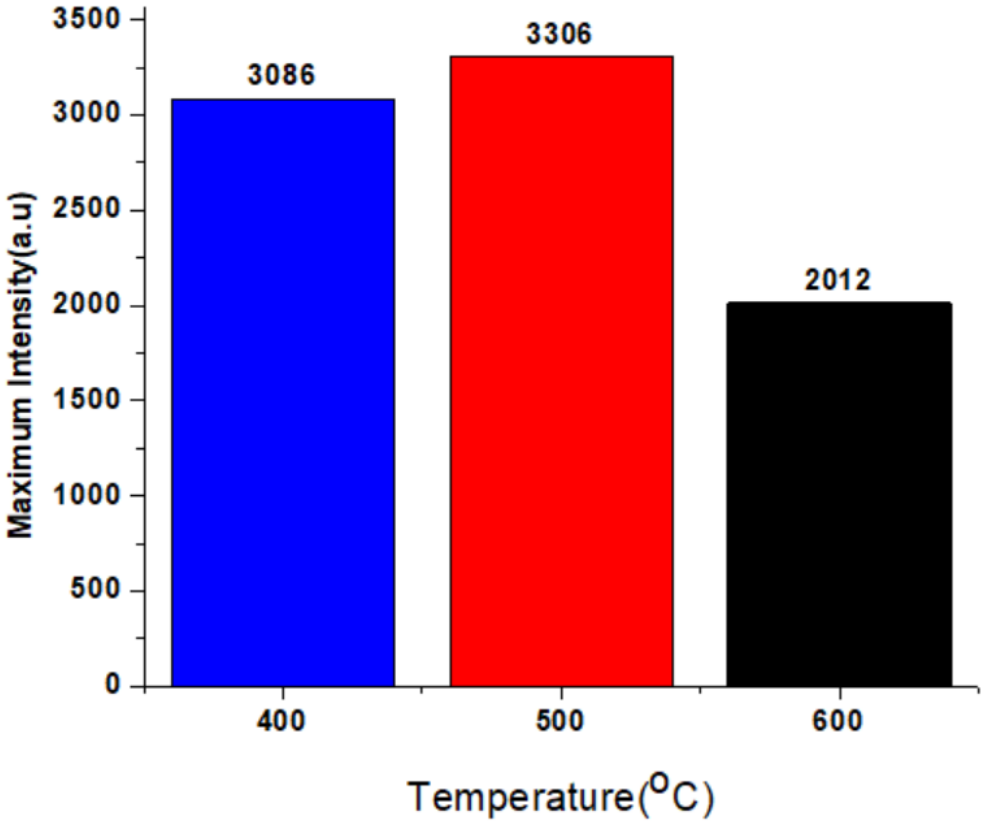

Figure 10: Maximum Intensity in XRD patterns of carbon for different temperatures.

As shown in the graph, the activated carbon having the best surface area and pore volume has the highest intensity and it's value is 3306 arbitrary units. Other samples of the carbon have comparatively low maximum intensity.

4.4 Fourier Transform-Infrared(FTIR)

Fourier Transform-Infrared (FTIR) Spectroscopy was used to detect the surface functional groups of the prepared activated carbon from Amla seed stones. FT-IR spectra of the prepared AC showed the major absorption band at 1056 cm^{-1} and 2952 cm^{-1} respectively. The band at 2952 cm^{-1} was assigned to –OH stretching of carboxyl, phenol and alcohol vibration and adsorbed water As the temperature of activation is increased the - OH functional group peak is shown to decrease and continuously disappear as in sample S_{600} which is at a temperature of 600 degrees. The fingerprint region verifies the synthesis of AC and the functional group region shows the continuous disappearance with an increase in temperature. The results of this FTIR analysis is in agreement to the analysis done by other researchers.

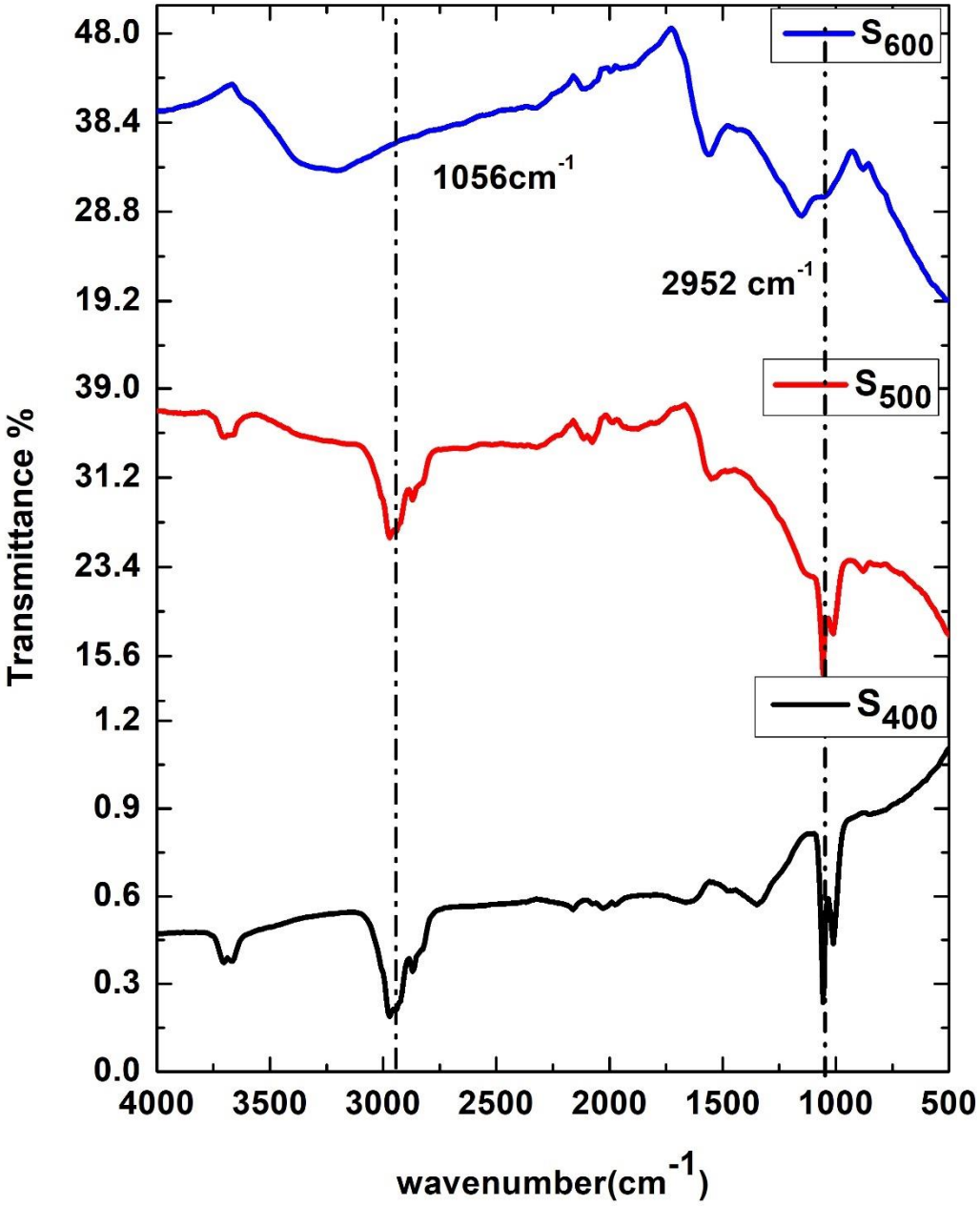

Figure 11: FTIR spectra of all the carbon samples

4.5 Raman Spectroscopy

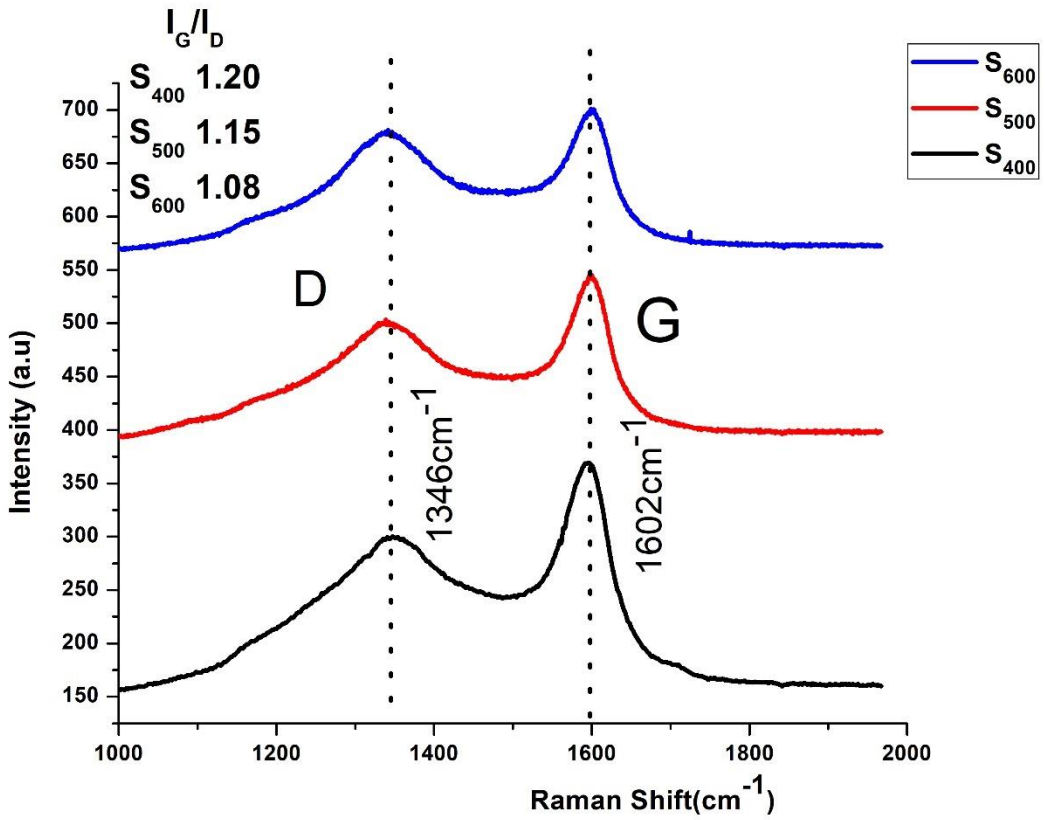

Figure 12: Raman Spectroscopy of the different samples of AC

The figure shows the Raman spectra of the synthesized ACs revealing strong D and G bands at approximately 1346 cm^{-1} and 1602 cm^{-1} respectively. The peak intensity ratio of the two bands i.e. G band and the D band helps us know about the crystallization of graphitic carbon in the synthesized sample. The ratio was found to be approximately equal to 1 in all the ACs confirming the formation of carbon of disordered structure. As the activation temperature increased, the sample shows a more amorphous nature. i.e., disorder increases. Moreover, the sample S_{600} shows the most amorphous naure i.e it is most suitable for the energy storage applications.

4.6 Scanning Electron Microscopy

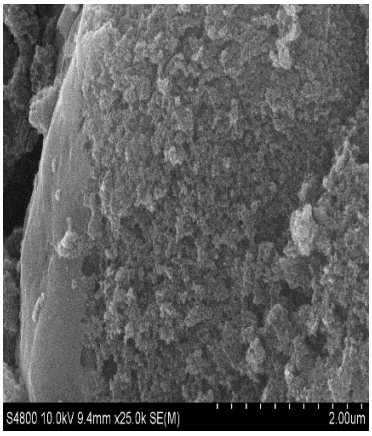

Figure 13: SEM image of sample S_{400}

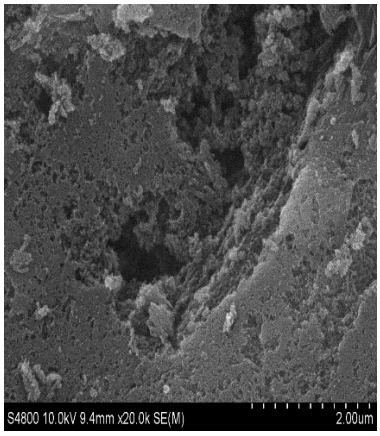

Figure 14: SEM image of sample S_{500}

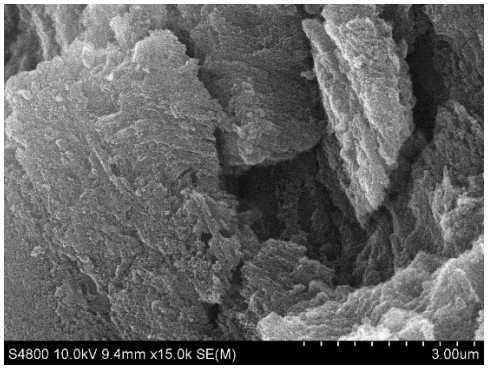

Figure 15: SEM image of sample S_{600}

The SEM images of the ACs at different temperatures show the microporous nature of the AC. The pore volume distribution is consistent with these electron micrographs. As the temperature is increased, we can see that the pore size increases and the carbon is suitable for energy storage application purposes.

4.7 Surface Area

The figure shows the surface area of the AC at different temperatures. The surface area varies from 722 to 844 m^2gm^{-1}. The AC synthesized at 500°C had the highest surfac8e area of 844 m^2/gm. As the surface area of the AC increases there is more

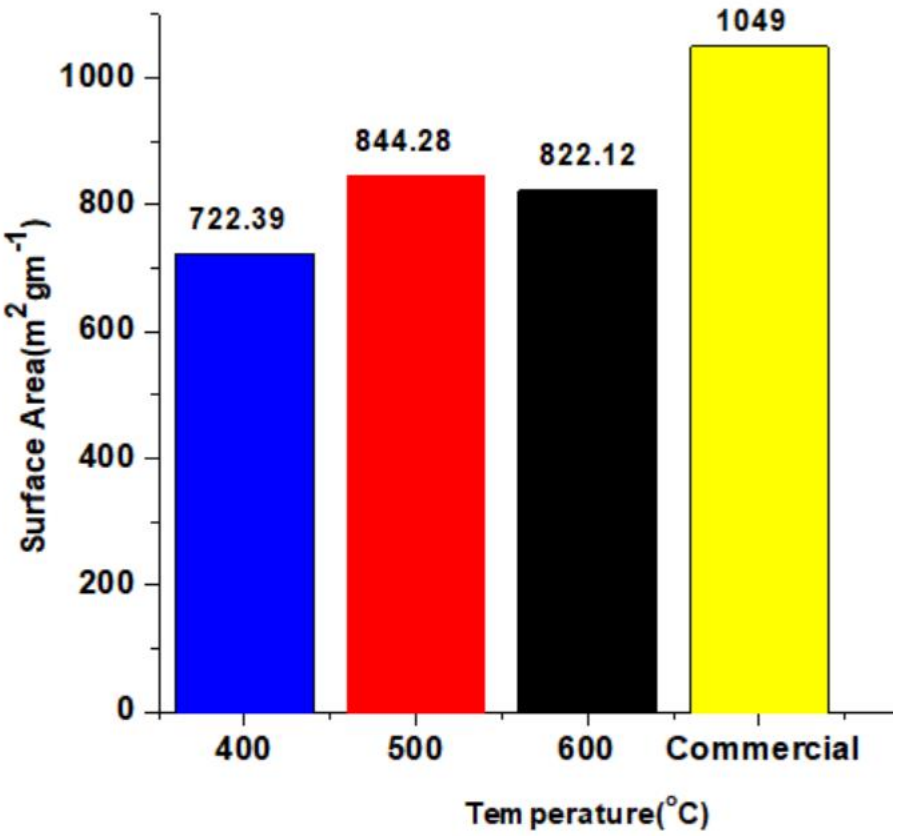

Figure 16: Surface Area of the ACs at different temperature of carbonization

4.8 Micropore Volume

The figure shows the micropore volume of the AC at different temperatures. The micropore volume varies from 0.39 to 0.57 cm^3gm^{-1}. The AC synthesized at 500 °C had the highest micropore volume of 0.57 cm^3gm^{-1}.

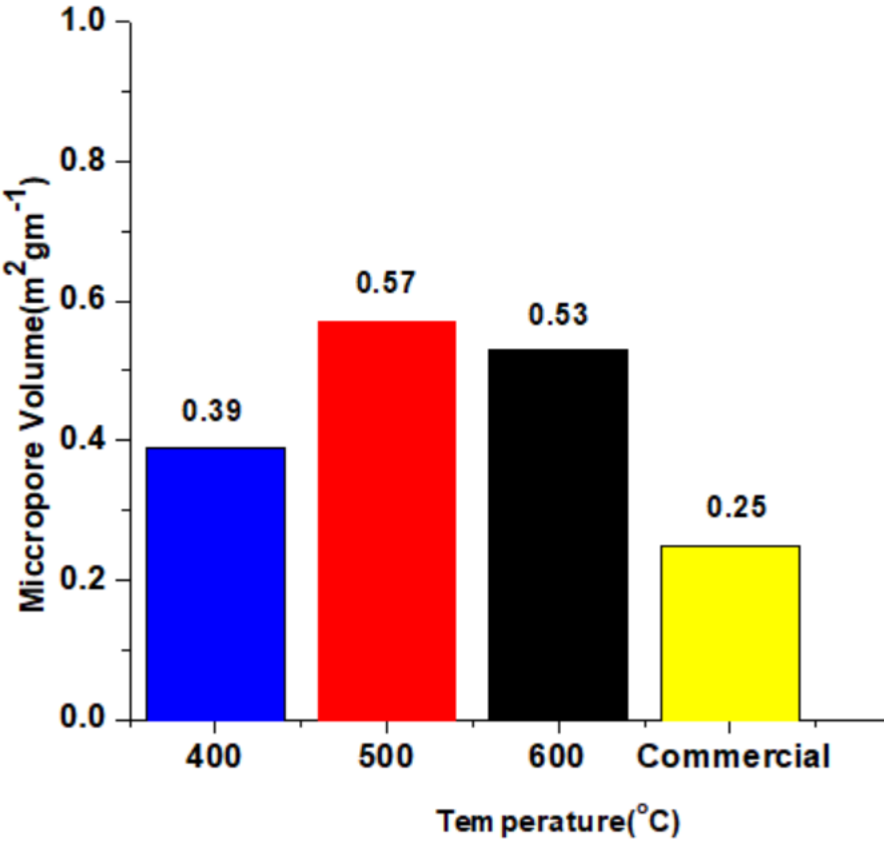

Figure 17: Micropore Volume of ACs at different temperature of carbonization

4.9 Total Pore Volume

The figure shows the total pore volume of the AC at different temperatures. The total pore volume varies from 0.68 to 0.81 cm^3gm^{-1}. The AC prepared at 500 °C had the highest total pore volume of 0.81 cm^3gm^{-1}

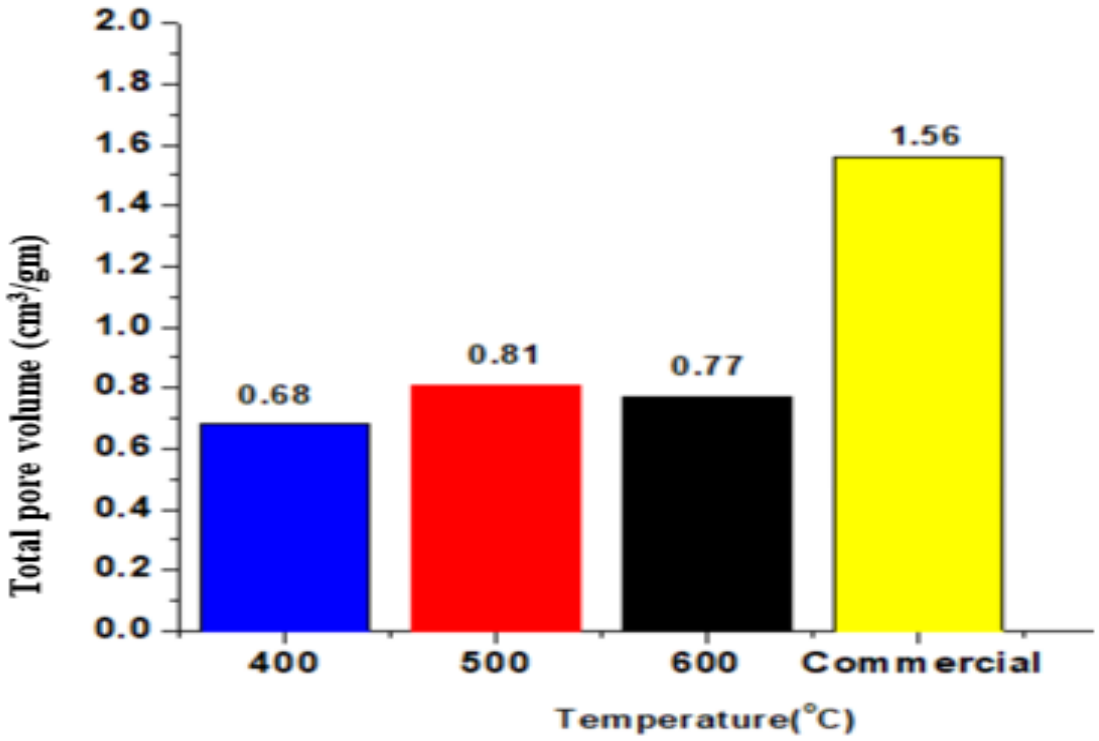

Figure 18: Total Pore Volume of different ACs at different temperature of carbonization.

4.10 Electrochemical Analysis of AC

The figure alongside shows the CV profile of the activated carbon at different temperatures. This measurement was done on scan rate of 5mV per seconds under the basic electrolyte of KOH and the area of voltammogram was calculated to calculate the specific capacitance.

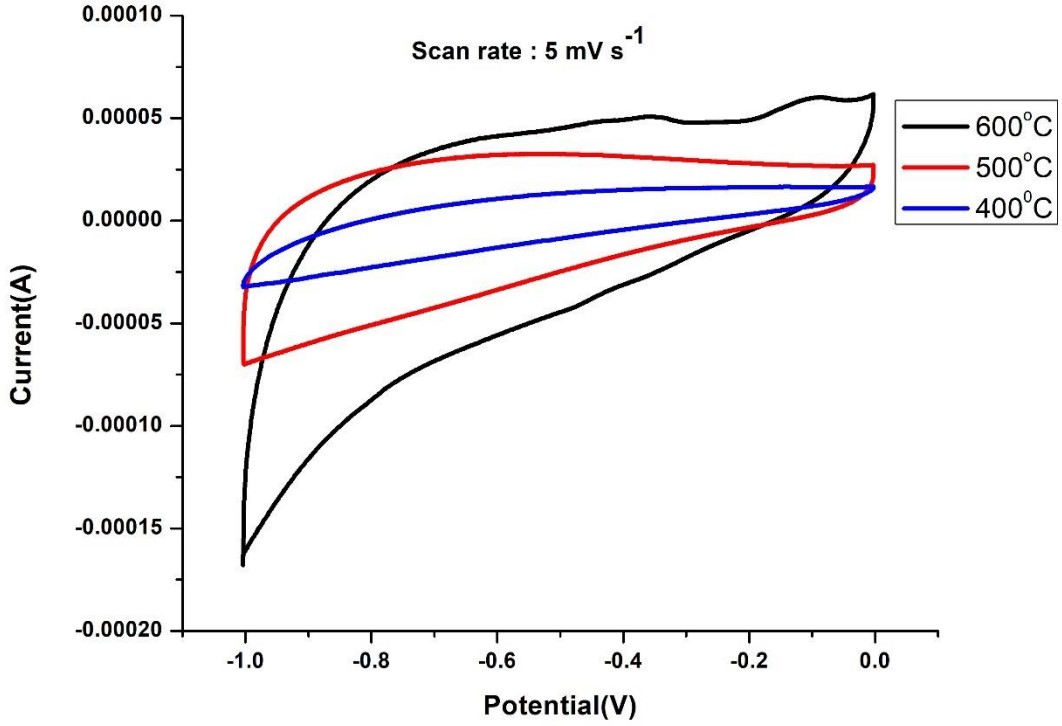

Figure 19 Voltammogram of S_{400}, S_{500}, S_{600} at 5 mVs^{-1}scan rate.

The specific capacitance is calculated to be Cp = 0.113Fcm^{-2} for S_{600} , 0.0729 Fcm^{-2} for S_{500} , 0.0251 Fcm^{-2} for S_{400} , according to the formula discussed in the methods. The voltammogram of the activated carbon sample prepared at different temperatures are shown below.

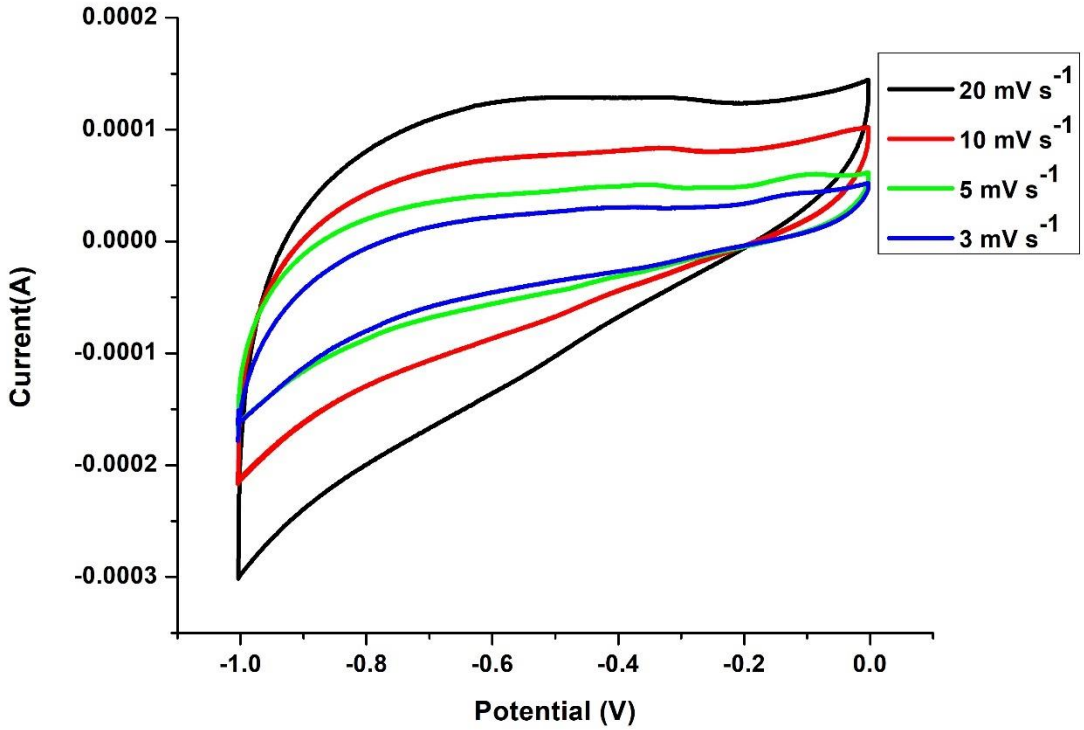

Figure 20 Voltammogram of S_{400}

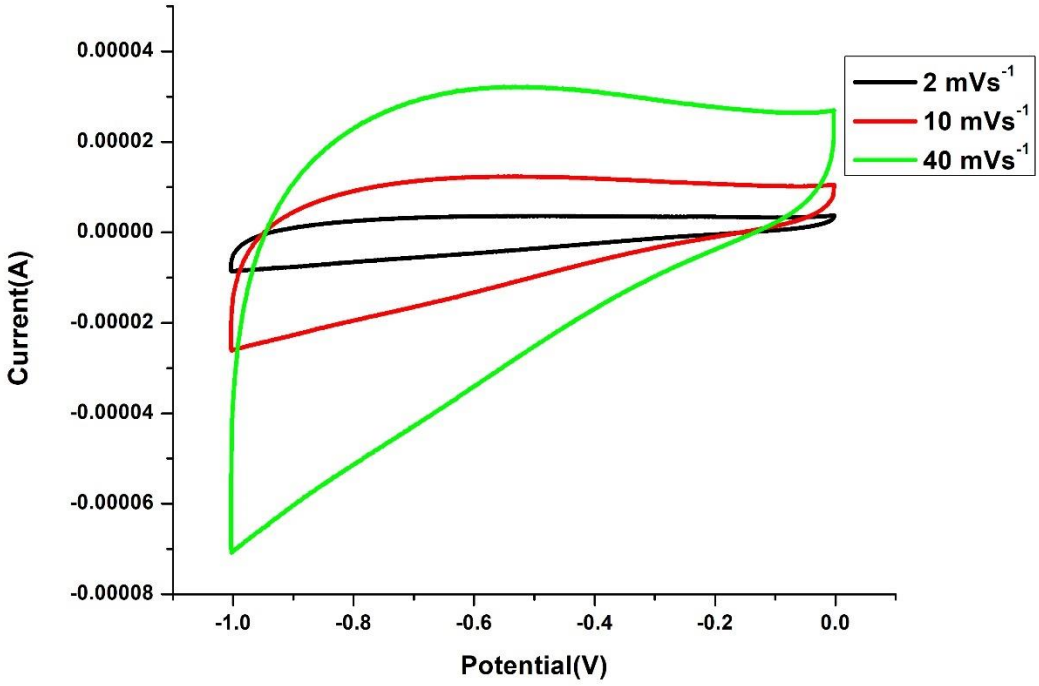

Figure 21 Voltammogram of S_{500}

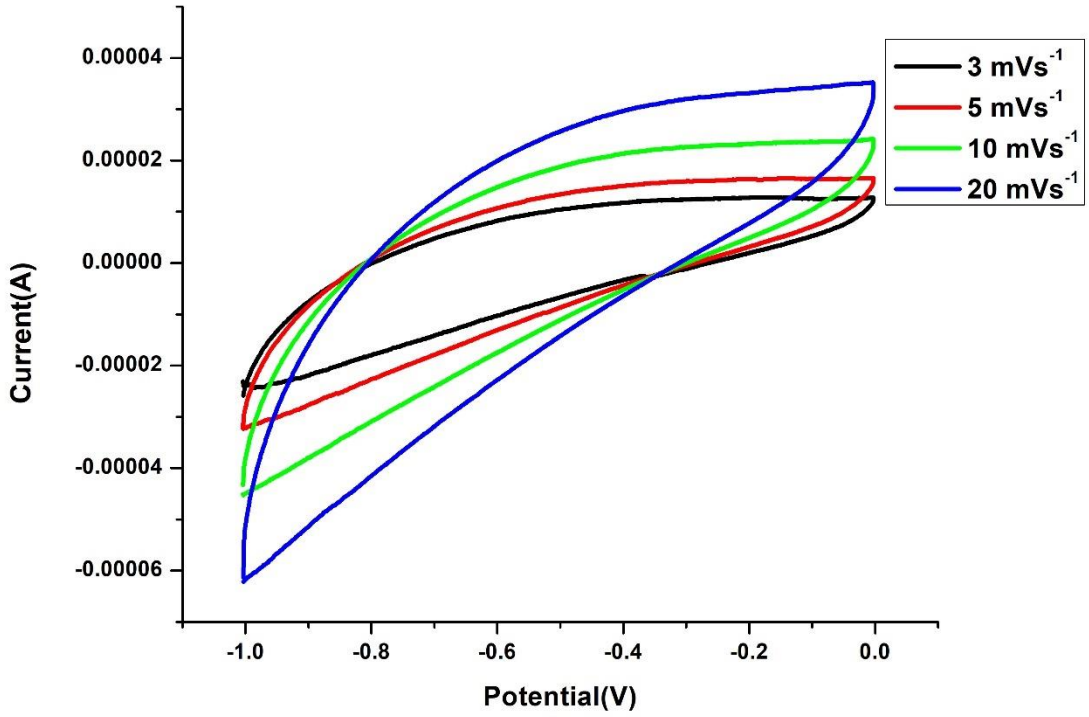

Figure 22 Voltammogram of S_{600}

An increasing scan rate caused the ions to move quickly towards the electrodes resulting in CV curve's leaf like shape. Since there were no redox peaks observed in the CV plot, the EDLC would be considered to have a capacitive property due to the ion accumulation between the electrodes rather than the ions being intercalated/deintercalated. The nature of the CV curve shows the prepared AC can form the double layer on its surface i.e. can be used as an EDLC supercapacitor.

4.10.1 Discussion

For the preparation of the AC, phosphoric acid was used as activating agent because zinc chloride harms the environment and KOH requires high temperature. Furthermore, phosphoric acid was readily available. The temperatures were chosen as 400 ^{o}C, 500 ^{o}C and 600 ^{o}C because of the data from thermogravimetric analysis (TGA). After the preparation of the samples their characterization revealed that the activated carbon formed at 500 degrees had the highest surface area as it's methylene blue number and iodine number were also highest. This sample had some functional groups as shown in FTIR. As the temperature increased, the peak of the functional groups gradually decreased. Moreover, the Xray diffraction also showed that this sample had the crystalline size of 95 Å at the temperature of carbonization temperature of 500 ^{o}C. In addition to this, the Raman spectroscopy revealed the G bands and D bands of the AC. The synthesized carbon was suitable for the supercapacitor application as the latter band (G band) was higher. The Cyclic voltammetry results showed that the activated carbon formed was suitable for energy storage applications as the CV curve was nearly rectangular and the specific capacitance for the high surface area sample was calculated to be Cp = 0.113Fcm^{-2} for S_{600} prepared at 600 ^{o}C..

5 CHAPTER FIVE: CONCLUSION AND RECOMMENDATION

5.1 Conclusion

Activated carbon was prepared from Amla seed stone by chemical activation with phosphoric acid in a ratio of 1:1 by weight at (400 - 600) °C for 4 hrs. The prepared activated carbon was characterized by methylene blue number, iodine number, surface area, total pore volume, XRD, FTIR, Raman, SEM and CV. The sample prepared at 500 degrees was found to have the methylene blue number and iodine number of the highest value i.e 307mg/g and 842 mg/g. Hence, this sample has the largest surface area of 844.28 m^2 per gm. The highest specific capacitance of the electrode from the samples was found to be Cp = 0.113Fcm^{-2} for $S_{600.}$. Hence, although the micropores for the sample prepared at 500 ^oC was found higher it doesn't necessarily mean it is suitable for energy storage application because for the transfer of ions and adsorption we need slightly bigger pores like the mesopores hence the sample prepared at 600 ^oC may have shown better electrochemical performance. i.e., high specific capacitance. The cyclic voltammetry graph along with the specific capacitance value shows that the prepared activated carbon can be used for energy storage applications. i..e electrode for supercapacitor. Moreover, the range of error for the second and the third sample overlap and hence may be cause of the discrepancy between the surface area and the specific capacitance of the samples. Though the data was compared with the commercial carbon (LEE et al., 2007), our samples had comparatively less value but it was near to the desired value.

5.2 Recommendation For Future Work

- BET method of calculation of surface area is preferred.
- Galvanostatic Charge Discharge (GCD) analysis can be done.
- Electrochemical Impedance Spectroscopy of the sample can be performed.

REFERENCES

Ahmad, T., & Zhang, D. (2020). A critical review of comparative global historical energy consumption and future demand: The story told so far. *Energy Reports*, *6*, 1973–1991. https://doi.org/10.1016/j.egyr.2020.07.020

Ali, A., Chiang, Y. W., & Santos, R. M. (2022). X-ray Diffraction Techniques for Mineral Characterization: A Review for Engineers of the Fundamentals, Applications, and Research Directions. *Minerals*, *12*(2), Article 2. https://doi.org/10.3390/min12020205

Arto, I., Capellán-Pérez, I., Lago, R., Bueno, G., & Bermejo, R. (2016). The energy requirements of a developed world. *Energy for Sustainable Development*, *33*, 1–13. https://doi.org/10.1016/j.esd.2016.04.001

Beguin, F., & Frackowiak, E. (2013). *Supercapacitors: Materials, Systems, and Applications*. John Wiley & Sons.

Berthomieu, C., & Hienerwadel, R. (2009). Fourier transform infrared (FTIR) spectroscopy. *Photosynthesis Research*, *101*(2), 157–170. https://doi.org/10.1007/s11120-009-9439-x

Chen, M., Kang, X., Wumaier, T., Dou, J., Gao, B., Han, Y., Xu, G., Liu, Z., & Zhang, L. (2013). Preparation of activated carbon from cotton stalk and its application in supercapacitor. *Journal of Solid State Electrochemistry*, *17*(4), 1005–1012. https://doi.org/10.1007/s10008-012-1946-6

Choi, J.-H. (2010). Fabrication of a carbon electrode using activated carbon powder and application to the capacitive deionization process. *Separation and Purification Technology*, *70*(3), 362–366. https://doi.org/10.1016/j.seppur.2009.10.023

Das, A., & Guo, H. (2022). Raman spectroscopy. In *Reference Module in Earth Systems and Environmental Sciences*. https://doi.org/10.1016/B978-0-12-822974-3.00031-8

Du, W., Wang, X., Ju, X., Xu, K., Gao, M., & Zhang, X. (2017). Carbonized Enteromorpha prolifera with porous architecture and its polyaniline composites as high-performance electrode materials for supercapacitors. *Journal of Electroanalytical Chemistry*, *802*, 15–21. https://doi.org/10.1016/j.jelechem.2017.08.044

Figueiredo, J. L., Pereira, M. F. R., Freitas, M. M. A., & Órfão, J. J. M. (1999). Modification of the surface chemistry of activated carbons. *Carbon*, *37*(9), 1379–1389. https://doi.org/10.1016/S0008-6223(98)00333-9

Frackowiak, E. (2013). *Supercapacitors: Materials, Systems, and Applications* (pp. 207–237). https://doi.org/10.1002/9783527646661.ch6

Gallo, A. B., Simões-Moreira, J. R., Costa, H. K. M., Santos, M. M., & Moutinho dos Santos, E. (2016). Energy storage in the energy transition context: A technology review. *Renewable and Sustainable Energy Reviews*, *65*, 800–822. https://doi.org/10.1016/j.rser.2016.07.028

Haimour, N. M., & Emeish, S. (2006). Utilization of date stones for production of activated carbon using phosphoric acid. *Waste Management*, *26*(6), 651–660. https://doi.org/10.1016/j.wasman.2005.08.004

Helseth, L. E. (2021). Comparison of methods for finding the capacitance of a supercapacitor. *Journal of Energy Storage*, *35*, 102304. https://doi.org/10.1016/j.est.2021.102304

Husien, S., El-taweel, R. M., Salim, A. I., Fahim, I. S., Said, L. A., & Radwan, A. G. (2022). Review of activated carbon adsorbent material for textile dyes removal: Preparation, and

modelling. *Current Research in Green and Sustainable Chemistry*, *5*, 100325. https://doi.org/10.1016/j.crgsc.2022.100325

Jagtoyen, M., & Derbyshire, F. (1993). Some considerations of the origins of porosity in carbons from chemically activated wood. *Carbon*, *31*(7), 1185–1192. https://doi.org/10.1016/0008-6223(93)90071-H

Joshi, S., Shrestha, L., Kamachi, Y., Yamauchi, Y., Adhikari Pradhananga, M., Pokharel, B., Ariga, K., & Pradhananga, R. (2015). Sodium Hydroxide Activated Nanoporous Carbons Based on Lapsi Seed Stone. *Journal of Nanoscience and Nanotechnology Vol. 15, 1465–1472, 2015*, *15*, 1465–1472. https://doi.org/10.1166/jnn.2015.9033

Karapınar, H. S. (2022). Adsorption performance of activated carbon synthesis by ZnCl2, KOH, H3PO4 with different activation temperatures from mixed fruit seeds. *Environmental Technology*, *43*(9), 1417–1435. https://doi.org/10.1080/09593330.2021.1968507

LEE, H.-H., HIRANO, Y., MURAYAMA, N., MATSUMOTO, S., & Shibata, J. (2007). Adsorption Properties of Activated Carbon Prepared from Waste Beer Lees by KOH Activation and CO2 Activation. *Resources Processing*, *54*, 19–24. https://doi.org/10.4144/rpsj.54.19

Li, L., Quinlivan, P. A., & Knappe, D. R. U. (2002). Effects of activated carbon surface chemistry and pore structure on the adsorption of organic contaminants from aqueous solution. *Carbon*, *40*(12), 2085–2100. https://doi.org/10.1016/S0008-6223(02)00069-6

Li, Q., Mahmood, N., Zhu, J., Hou, Y., & Sun, S. (2014). Graphene and its composites with nanoparticles for electrochemical energy applications. *Nano Today*, *9*(5), 668–683. https://doi.org/10.1016/j.nantod.2014.09.002

Lignocellulosic biomass processing: A perspective. (n.d.). Retrieved September 11, 2022, from https://www.cabdirect.org/cabdirect/abstract/20043043925

Lim, K. O. (1996). CHARCOAL AND GLUCOSE/ETHANOL PRODUCTION FROM OIL PALM AND COCOA PLANTATION WASTES. In P. Chartier, G. L. Ferrero, U. M. Henius, S. Hultberg, J. Sachau, & M. Wiinblad (Eds.), *Biomass for Energy and the Environment* (pp. 1516–1521). Pergamon. https://doi.org/10.1016/B978-0-08-042849-9.50012-4

Liu, Y., Wu, Q., Lingyang, L., Pantrangi, M., Kang, L., & Ran, F. (2020). Anode Material of Vanadium Nitride for Supercapacitors: A Topic Review. *Journal of Materials Chemistry A*, *8*. https://doi.org/10.1039/D0TA01490G

Ma, H., Wang, L., Feng, X., Chen, Y., Wu, J., Zhao, M., & Zhou, J. (2021). Are activated carbon pore structure parameters linearly positively related to its mass-specific capacitance? *Journal of Materials Science*, *56*(21), 12336–12349. https://doi.org/10.1007/s10853-021-06106-7

Ma, R., Qin, X., Liu, Z., & Fu, Y. (2019). Adsorption Property, Kinetic and Equilibrium Studies of Activated Carbon Fiber Prepared from Liquefied Wood by Zncl2 Activation. *Materials*, *12*(9), 1377. https://doi.org/10.3390/ma12091377

Mallick, A., Jha, A., Pokharel, B., Rajbhandari, R., & Shrestha, R. (2019). Activated Carbons Derived from Date (Phoenix dactylifera) Seeds with Excellent Iodine Adsorption Properties. *Journal of the Institute of Engineering*, *15*, 165–170. https://doi.org/10.3126/jie.v15i2.27663

Marsh, H., & Reinoso, F. R. (2006). *Activated Carbon*. Elsevier.

Mehta, S., Jha, S., & Liang, H. (2020). Lignocellulose materials for supercapacitor and battery electrodes: A review. *Renewable and Sustainable Energy Reviews*, *134*, 110345. https://doi.org/10.1016/j.rser.2020.110345

Mianowski, A., Owczarek, M., & Marecka, A. (2007). Surface Area of Activated Carbon Determined by the Iodine Adsorption Number. *Energy Sources, Part A: Recovery, Utilization, and Environmental Effects*, *29*(9), 839–850. https://doi.org/10.1080/00908310500430901

Mozhiarasi, V., & Natarajan, T. S. (2022). Bael fruit shell–derived activated carbon adsorbent: Effect of surface charge of activated carbon and type of pollutants for improved adsorption capacity. *Biomass Conversion and Biorefinery*. https://doi.org/10.1007/s13399-022-03211-8

Mukhiya, T., Dahal, B., Ojha, G. P., Kang, D., Kim, T., Chae, S.-H., Muthurasu, A., & Kim, H. Y. (2019). Engineering nanohaired 3D cobalt hydroxide wheels in electrospun carbon nanofibers for high-performance supercapacitors. *Chemical Engineering Journal*, *361*, 1225–1234. https://doi.org/10.1016/j.cej.2019.01.006

Naji, S. Z., & Tye, C. T. (2022). A review of the synthesis of activated carbon for biodiesel production: Precursor, preparation, and modification. *Energy Conversion and Management: X*, *13*, 100152. https://doi.org/10.1016/j.ecmx.2021.100152

Nunes, C., & Guerreiro, M. (2011). Estimation of surface area and pore volume of activated carbons by methylene blue and iodine numbers. *Quimica Nova*, *34*, 472–476. https://doi.org/10.1590/S0100-40422011000300020

Olabi, A. G., Onumaegbu, C., Wilberforce, T., Ramadan, M., Abdelkareem, M. A., & Al – Alami, A. H. (2021). Critical review of energy storage systems. *Energy*, *214*, 118987. https://doi.org/10.1016/j.energy.2020.118987

Oyedotun, K. (2018). *Synthesis and characterization of carbon-based nanostructured material electrodes for designing novel hybrid supercapacitors*. https://doi.org/10.13140/RG.2.2.20007.50084

Pandolfo, T., Ruiz, V., Sivakkumar, S., & Nerkar, J. (2013). General Properties of Electrochemical Capacitors. In *Supercapacitors* (pp. 69–109). John Wiley & Sons, Ltd. https://doi.org/10.1002/9783527646661.ch2

Pani, A., Shirkole, S. S., & Mujumdar, A. S. (2022). Importance of renewable energy in the fight against global climate change. *Drying Technology*, *0*(0), 1–2. https://doi.org/10.1080/07373937.2022.2119324

Raaf, A., Suriaini, N., Djafar, F., Syamsuddin, Y., & Supardan, M. (2021a). Effect of drying temperature on the moisture loss, acidity and characteristics of Amla fruit. *IOP Conference*

Series: Earth and Environmental Science, *667*(1), 012047. https://doi.org/10.1088/1755-1315/667/1/012047

Raaf, A., Suriaini, N., Djafar, F., Syamsuddin, Y., & Supardan, M. D. (2021b). Effect of drying temperature on the moisture loss, acidity and characteristics of Amla fruit. *IOP Conference Series: Earth and Environmental Science*, *667*(1), 012047. https://doi.org/10.1088/1755-1315/667/1/012047

Rajabathar, J. R., Sivachidambaram, M., Vijaya, J. J., Al-lohedan, H. A., & Aldhayan, D. M. D. (2020). Flexible type symmetric supercapacitor electrode fabrication using phosphoric acid-activated carbon nanomaterials derived from cow dung for renewable energy applications. *ACS Omega*, *5*(25), 15028–15038. https://doi.org/10.1021/acsomega.0c00848

Rajapaksha, H. G. N., Meghapathirana, N., Perera, K. S., & Vidanapathirana, K. P. (2022). Cost-effective, environmental friendly electrochemical double-layer capacitor with an optimized electrode composition. *Journal of Materials Science: Materials in Electronics*, *33*(15), 11794–11801. https://doi.org/10.1007/s10854-022-08143-7

Ratajczak, P., Suss, M. E., Kaasik, F., & Béguin, F. (2019). Carbon electrodes for capacitive technologies. *Energy Storage Materials*, *16*, 126–145. https://doi.org/10.1016/j.ensm.2018.04.031

Ritchie, H., Roser, M., & Rosado, P. (2020). Energy. *Our World in Data*. https://ourworldindata.org/energy-mix

Şahin, Ö., Saka, C., Ceyhan, A. A., & Baytar, O. (2015). Preparation of High Surface Area Activated Carbon from Elaeagnus angustifolia Seeds by Chemical Activation with ZnCl2 in

One-Step Treatment and its Iodine Adsorption. *Separation Science and Technology*, *50*(6), 886–891. https://doi.org/10.1080/01496395.2014.966204

Saini, R., Sharma, N., Oladeji, O. S., Sourirajan, A., Dev, K., Zengin, G., El-Shazly, M., & Kumar, V. (2022). Traditional uses, bioactive composition, pharmacology, and toxicology of Phyllanthus emblica fruits: A comprehensive review. *Journal of Ethnopharmacology*, *282*, 114570. https://doi.org/10.1016/j.jep.2021.114570

Shafiei, N., Nasrollahzadeh, M., & Hegde, G. (2021). Chapter 10—Biopolymer-based (nano)materials for supercapacitor applications. In M. Nasrollahzadeh (Ed.), *Biopolymer-Based Metal Nanoparticle Chemistry for Sustainable Applications* (pp. 609–671). Elsevier. https://doi.org/10.1016/B978-0-323-89970-3.00010-X

Shiratori, N., Lee, K., Miyawaki, J., Hong, S.-H., Mochida, I., An, B., Yokogawa, K., Jang, J., & Yoon, S.-H. (2009). Pore Structure Analysis of Activated Carbon Fiber by Microdomain-Based Model. *Langmuir*, *25*(13), 7631–7637. https://doi.org/10.1021/la9000347

Shrestha, D., & Rajbhandari, A. (2021). The effects of different activating agents on the physical and electrochemical properties of activated carbon electrodes fabricated from wood-dust of Shorea robusta. *Heliyon*, *7*(9), e07917. https://doi.org/10.1016/j.heliyon.2021.e07917

Sivachidambaram, M., Vijaya, J. J., Kennedy, L. J., Jothiramalingam, R., Al-Lohedan, H. A., Munusamy, M. A., Elanthamilan, E., & Merlin, J. P. (2017). Preparation and characterization of activated carbon derived from the Borassus flabellifer flower as an electrode material for supercapacitor applications. *New Journal of Chemistry*, *41*(10), 3939–3949. https://doi.org/10.1039/C6NJ03867K

Somasundaran, P. (2006). *Encyclopedia of Surface and Colloid Science*. CRC Press.

Staveley, L. A. K. (2016). *The Characterization of Chemical Purity: Organic Compounds*. Elsevier.

Tyagi, A., & Gupta, R. (2015). *Carbon Nanostructures from Biomass Waste for Supercapacitor Applications*. https://doi.org/10.1201/b19168-11

Tyagi, A., Mishra, K., Sharma, S. K., & Shukla, V. K. (2022). Performance studies of an electric double-layer capacitor (EDLC) fabricated using edible oil-derived activated carbon. *Journal of Materials Science: Materials in Electronics*, *33*(11), 8920–8934. https://doi.org/10.1007/s10854-021-06978-0

Üner, O., & Bayrak, Y. (2018). The effect of carbonization temperature, carbonization time and impregnation ratio on the properties of activated carbon produced from Arundo donax. *Microporous and Mesoporous Materials*, *268*, 225–234. https://doi.org/10.1016/j.micromeso.2018.04.037

Veeramani, V., Sivakumar, M., Chen, S.-M., Madhu, R., R. Alamri, H., A. Alothman, Z., A. Hossain, M. S., Chen, C.-K., Yamauchi, Y., Miyamoto, N., & C.-W. Wu, K. (2017). Lignocellulosic biomass-derived, graphene sheet-like porous activated carbon for electrochemical supercapacitor and catechin sensing. *RSC Advances*, *7*(72), 45668–45675. https://doi.org/10.1039/C7RA07810B

Wang, C., & Gu, C. (2022). X-Ray Diffraction. In *Reference Module in Earth Systems and Environmental Sciences*. https://doi.org/10.1016/B978-0-12-822974-3.00037-9

Williams, P. T., & Reed, A. R. (2006). Development of activated carbon pore structure via physical and chemical activation of biomass fibre waste. *Biomass and Bioenergy*, *30*(2), 144–152. https://doi.org/10.1016/j.biombioe.2005.11.006

Yahya, M. A., Al-Qodah, Z., & Ngah, C. W. Z. (2015). Agricultural bio-waste materials as potential sustainable precursors used for activated carbon production: A review. *Renewable and Sustainable Energy Reviews*, *46*, 218–235. https://doi.org/10.1016/j.rser.2015.02.051

Yu, A., Chabot, V., & Zhang, J. (2017). *Electrochemical Supercapacitors for Energy Storage and Delivery: Fundamentals and Applications*. CRC Press.

APPENDIX A: PHOTOS TAKEN DURING THE RESEARCH WORK

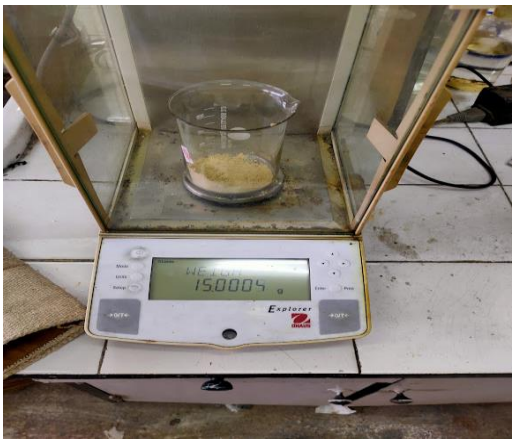


MARINE INDIA
ROTARY SHAKER
2058